Characterization of the Boulder Front Fault and Uplift Rates in the Northern Basin and Range Province, Idaho

Characterization of the Boulder Front Fault and Uplift Rates in the Northern Basin and Range Province, Idaho

by

Sedona Boyle

Presented to the Graduate and Research Committee of Lehigh University in Candidacy for the Degree of Master of Science

in

Earth and Environmental Sciences

Lehigh University

January 2025

Thesis is accepted and approved in partial fulfillment of the requirements for the Master of Science in Earth and Environmental Sciences

Sedona Boyle

Date Approved: 11/26/2024

List of Committee Members: Dr. David Anastasio, Dr. Frank Pazzaglia, Dr. Claudio Berti

Acknowledgements

Funding for this project was provided by the EDMAP Program of the National Cooperative Geologic Mapping Program of the US Geological Survey under Grant Number G22AC00177, a Geological Society of America Graduate Student Research Grant and the Lehigh EES Palmer Fund. A huge thank you to Dr. David Anastasio for serving as my advisor for the past 2.5 years and for providing valuable advice throughout my time in graduate school. Thank you to Dr. Claudio Berti for advising work with the EDMAP project and sharing excellent field knowledge. A special thanks to Tabitha Nowak for her field assistance throughout two field seasons in Idaho and Dr. Frank Pazzaglia for advising the uplift modeling and sharing helpful comments as a member of my committee. Thank you to Dr. Christine Regalla for the aid with the MATLAB diffusion code and Sarah Truxal for gathering the preliminary data for this project in 2021. Thank you to the Idaho Geological Survey for providing the GNSS equipment used to make the profiles and for funding the radiocarbon data. A final massive thank you to my family, friends, and the Lehigh EES department for inspiring my passion for the Earth and nature.

Table of Contents

List of Tables

List of Figures

Abstract

The Northern Basin and Range Province in central Idaho is host to a series of active normal faults including the range-bounding Boulder Front fault along the SW slope of the Boulder Mountains. Situated in the upper Wood River watershed, the SW-dipping Boulder Front fault cuts a series of Pinedale-age moraines and fluvial outwash terraces with clear evidence of surficial rupture. At least 7 distinct fault segments dip ~SW and span more than 20 kilometers from Galena Summit to the SE of Boulder Creek. Evidence of multiple ruptures of the entire segment during the Holocene is observed with inset deposits being less offset than older terraces. Rupture ages were calculated from diffusion modeling of the fault scarp as a single slip rupture event (~4.27-7.08kyr±0.68kyr) and a continuous slip event (~2.99-4.96kyr±0.41kyr) with additional constraints provided by six radiocarbon dates (~1.12-4.48kyr±0.06kyr) in the footwall of offset fluvial terrace deposits. A recent rupture (<~2.81kyr±0.06kyr) is evident on the Boulder Creek segment while neighboring drainages suggest that other segments of the Boulder Front fault may have ruptured within the last ~1,100 years. Calibration of a diffusion coefficient for glacial sediment near Boulder Creek was determined locally to be 2.09×10^{-3} m^2/yr. Recurrence intervals of ~2.3kyr and earthquakes of M5.7-M6.6 are calculated for the Boulder Front fault based on rupture-length relationships, diffusional modeling, and radiometric dating techniques. Erosion rates calculated from ^{10}Be analysis and corresponding uplift rates from fluvial inversion modeling for regional catchments reveal that catchments with fault scarps have 3.5-4 times higher uplift rates than catchments with no visible scarps. Physical extension of the fault system may exist to the south towards the tourist destinations of Ketchum and Sun Valley, Idaho, and poses a seismic hazard to infrastructure and local populations.

1. Introduction

Faults scarps, visible offsets in the topography of a tectonically altered landscape, serve as geologic markers of historical ground-rupturing earthquakes. The active extension of the crust in the Northern Basin and Range Province is characterized by the development of NW-trending normal faults (Regalla et al., 2007; Anastasio et al., 2010). Normal faults producing earthquakes shallow enough or with high enough magnitudes to rupture the ground surface leave observable fault scarps creating a clear shift between the hanging wall and the footwall of recent faults. The separation between these fault blocks produces the fault scarp, a transient, steep topographic offset showing the expression of the fault plane at the Earth's surface (Stewart & Hanock, 1990). After formation, the slope of the scarp degrades through soil creep and can be modeled by diffusion (Nash, 1986; Matson & Bruhn, 2001). Modeling the post-rupture diffusional history of an older scarp provides insights into previous tectonic activity of the fault and informs seismic hazards.

Prime examples of the NW-trending range-bounding faults making up the Northern Basin and Range are the Quaternary, Class A Sawtooth and Boulder Front faults (Crone et al., 2010; Crone & Neier, 2010). The Boulder Front fault, bounding the Boulder Mountains to the south in the upper Wood River Valley, extends along strike from the ~60 km long Sawtooth fault to its NW (Figure 1; Thackray, 2013, Lifton et al., 2023). No surface linkage between these two faults has been observed in the field however, a polarity change is apparent across the valley between the NE-dipping Sawtooth fault to the SW-dipping Boulder Front fault. A possible seismogenic linkage zone exists between the two active faults near the accommodation zone of Galena Summit based on the accommodation of extension (Di Bucci et al., 2006; Liberty et al., 2021).

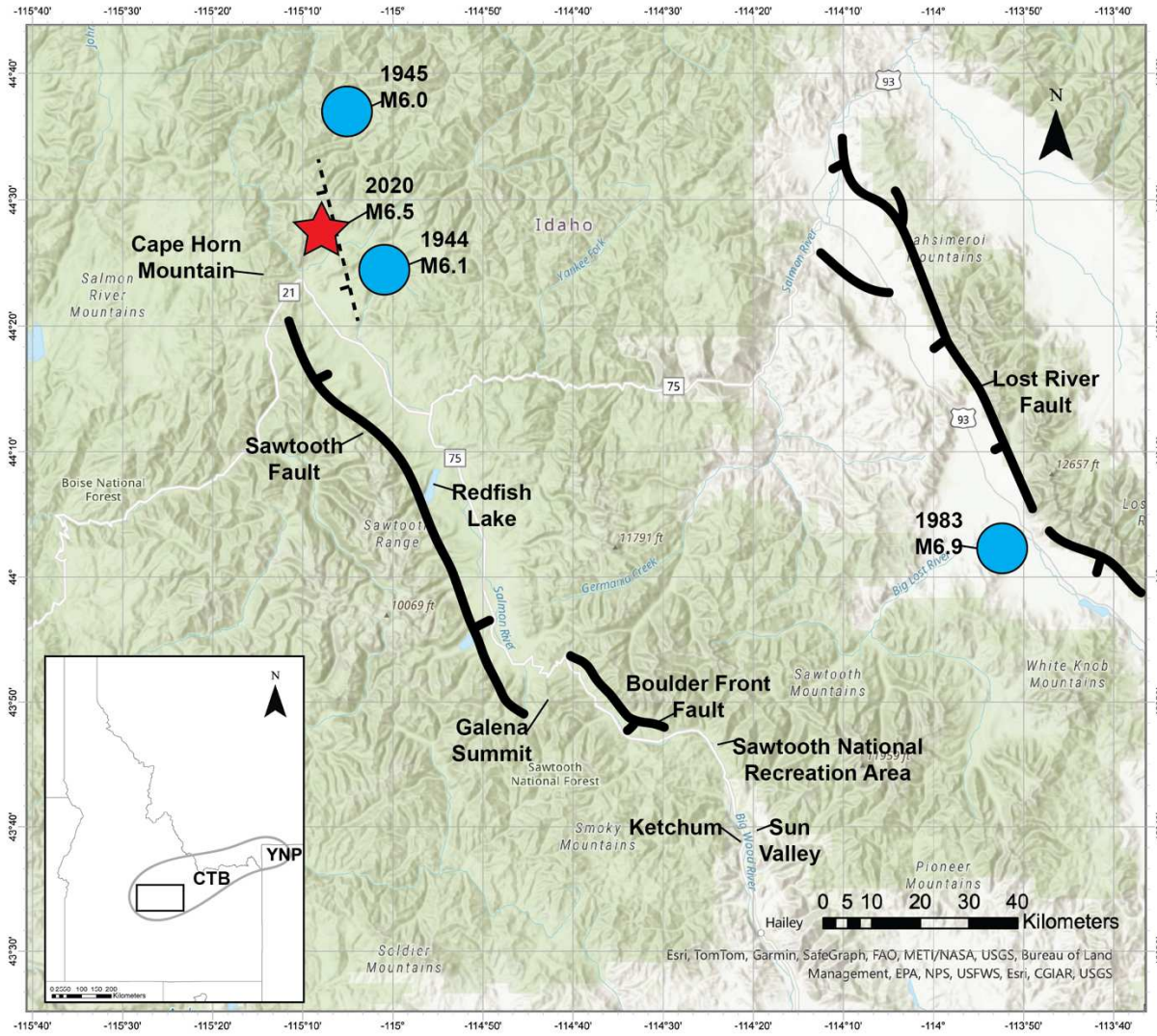

Figure 1. Map of central Idaho showing Quaternary, Class A faults from the USGS and significant historical earthquakes of M6.0 or greater. The red star denotes the M6.5 Stanley earthquake. The blue dots are the M6.0 and M6.1 Seafoam earthquakes and the M6.9 Borah Peak earthquake.

This thesis presents a newly interpreted surficial geologic map, results from fault scarp diffusion modeling, and radiometric dating to analyze the two most recent ruptures (Holocene and late Pleistocene), and extent of the Boulder Front fault. In addition, regional ^{10}Be terrestrial cosmogenic nuclide (TCN) data are used to model basin-averaged erosion rates that are subsequently used to invert the fluvial topography of the catchments and reconstruct the pre-late Pleistocene base-level fall history (Fisher et al., 2022).

Previous studies have reported the Boulder Front fault length to be 9 km but based on a Light Detecting and Ranging (LiDAR) digital elevation model (DEM) interpretation and small-scale field mapping, the Boulder Front fault is expressed at the surface by 7 distinct segments from Galena Summit towards just east of Boulder Creek, spanning over 20 km along strike (Crone & Neir, 2010; Boyle et al., 2023). Bare earth processing of the LiDAR data eliminates dense vegetation from imagery allowing fault scarps to be mapped in hard-to-access regions in this part of the Sawtooth National Forest. These fault segments are defined by their physical characteristics, geographic extent, and strike orientations with the longest fault segment, near Boulder Creek, measuring 2.2 km.

The Boulder Front fault is adjacent to the Sawtooth National Recreation Area and close to several renowned tourist venues in Idaho, creating a potential seismic hazard to the region. The M_w6.9 Borah Peak earthquake resulted in millions of dollars in property damage and two deaths as a result of infrastructure failing to withstand the earthquake's effects (Idaho Office of Emergency Management, 2019; Liberty et al., 2021). The Boulder Front fault poses a proximal threat to the towns of Ketchum and Sun Valley, Idaho, located less than 20 km SE of the fault (Figure 1). Residential homes and private businesses located at the foothills of these mountainous regions are susceptible to damage from ground shaking and landslides. Determination of the rupture history of faults in the Northern Basin and Range Province is essential to informing local populations on seismic hazards.

2. Geologic Setting

2.1. *Northern Basin and Range Province*

The inland western United States is primarily located in the "classic" Basin and Range Province which extends from southern Idaho to the southern parts of Arizona and New Mexico

(Osborn, 2024). Extension of the traditional system exists to the north in east and central Idaho and southwestern Montana, as well as to the south through parts of Mexico (Osborn, 2024). The Snake River Plain isolates the northern section from the rest of the geological province to the south (Gans & Bohrson, 1998; Newmann, 2019). The crustal extension in the Northern Basin and Range drives constant change of the landscape leading to the formation of subparallel mountain ranges and valleys (Stickney & Bartholomew, 1987; Osborn, 2024). A goal of this thesis is to better understand the role fault systems play in the uplift of mountain ranges in this area of active mantle upwelling (Liu & Shen, 1998). Basin and Range extension occurs at S45°W±15° and therefore faults are oriented perpendicular to the direction of highest strain at N45°W±15° (Stickney & Bartholomew, 1987).

The Sawtooth and Boulder Front faults fall within the western edge of the Centennial Tectonic Belt, an area of high seismicity in the western United States extending about 350 km long and 50-100 km wide in a zone parallel to the northern extent of the Snake River Plain from central Idaho to Yellowstone National Park (YNP) (Stickney & Bartholomew, 1987; Stickney 1993). Although YNP is associated with highly active volcanism, seismic refraction studies show the crust in the Centennial Tectonic Belt to be unaltered by the hotspot activity (Payne et al., 2013). The Centennial Tectonic Belt includes the Lost River Range and seismicity in both the Sawtooth Valley and upper Wood River Valley (Stickney & Bartholomew, 1987).

2.2. *Regional Earthquakes*

Surrounding regions of the Boulder Front fault segments have experienced four moderate to large earthquakes over the past 80 years (Figure 1). These seismic events are the 1944 M6.1 and 1945 M6.0 Seafoam earthquakes and the 1983 M_w6.9 Borah Peak earthquake, along with the most recent 2020 M6.5 Stanley earthquake, which occurred just north of the northern termination

of the Sawtooth fault scarp (Liberty et al., 2021). Ruptures in the ground surface were only observed in the eastern Lost River Valley following the Borah Peak earthquake, about 65 km to the NW of the Boulder Front fault. Previous studies reported that earthquakes of less than M6.0 would produce poor surface expression and inconsistencies if rupturing the ground surface of the Northern Basin and Range Province (Wells & Coppersmith, 1994). There is no reported ground rupture associated with the M6.5 Stanley earthquake, although regional ground displacement was imaged through InSAR analysis (Liberty et al., 2021)

2.3. *Glaciations*

Two major glaciations are apparent in the central Idaho landscapes. There is the Bull Lake glaciation that took place ~140 kyr and is defined by older, weathered moraines with wider ridges (Pierce, 2003). The most recent Pinedale glaciation peaked ~16 kyr ago and its moraines are less weathered and have taller and sharper ridges (Williams, 1961; Easterbrook et al., 2011).

Comprehensive glaciation studies were conducted ~50 km northwest of the Boulder Front fault at Redfish Lake (Figure 1). Although the studies were set north of Galena Summit in the Sawtooth Valley, moraines of similar morphology are seen in the upper Wood River Valley near the Boulder Front fault. Exposed scarps from late Pleistocene glacial deposits demonstrate offset in the lateral moraines of Boulder Creek due to seismic activity in the late Quaternary (<~15.76kyr) (Crone & Neier, 2010; Easterbrook et al., 2011). The physical offset and ages of these glacial landforms will be used to determine the rupture age and slip rate history of the Boulder Front fault. Additionally, glaciations shaped the landscape where several fault segments are located and may affect long-term erosion and uplift rates in regional catchments.

3. Faulting Analysis Methods and Results

The objective of the first part of the study is to present the characterization of the Boulder Front fault in terms of segments, rupture history, vertical offset, and slip rate. Through digital elevation model interpretation, radiocarbon dating, and diffusion modeling, the late Quaternary tectonic activity of this understudied fault is examined. Recurrence intervals and seismic hazards are then estimated for the Boulder Creek segment and the entire Boulder Front fault.

3.1. *Surficial Geologic Mapping*

During two field seasons in 2023 and 2024, a map of the surficial geology and Boulder Front fault was completed for parts of the Easley Hot Springs and Amber Lakes 7.5' quadrangles in central Idaho at a 1:12,000 scale (Figure 2 & Appendix A). Previous small-scale lithologic maps have been made for the area, however, there is no current map of the surficial geology. Mapping involved a combination of the surficial geology, lithology, and structural features, and was used to determine the relative stratigraphy of the surficial deposits.

Prior to fieldwork, a DEM was derived through bare earth processing of a LiDAR dataset (Idaho Lidar Consortium, 2021; IGS, personal communication, 2022). This processed model for initial interpretation of the field area was used to create a preliminary surficial geologic map of the Boulder Creek area and to determine the extent of the fault segments across the southern face of the Boulder Mountains. Topographic base maps with a contour interval of 10 m were made using the DEM for referencing during fieldwork. A compilation of the field mapping notes, acquired field data, and remote interpretation of DEM's was created in ArcGIS Pro 3.2.0 at a 1:24,000 scale (Appendix A).

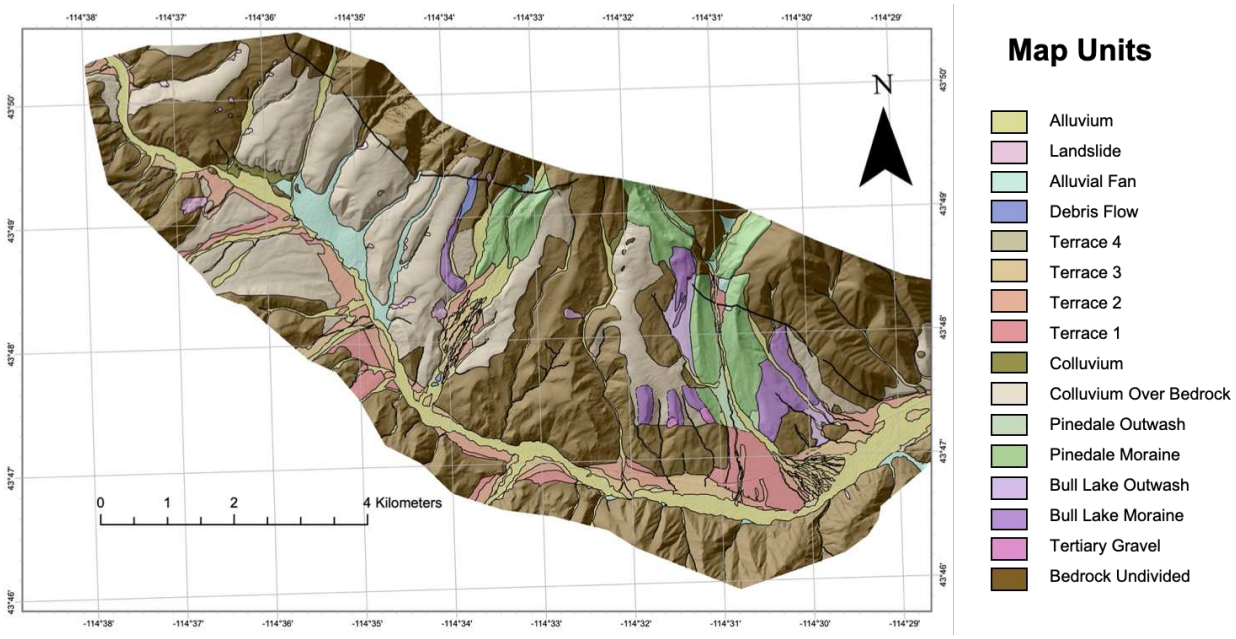

Figure 2. Mapped area of parts of Easley Hot Springs and Amber Lakes 7.5' quadrangles. Full 1:24,000 scale map and description in Appendix A.

3.1.1. *Surficial Units*

In the mapped area of the Easley Hot Springs and Amber Lakes 7.5' quadrangles, 16 different surficial units were observed (Figure 2; Figure 3). The morpho-stratigraphic relationships of the surficial geology were assembled from field notes, radiocarbon dating, and regional studies (Figure 3).

Among the alluvial deposits in the map area are the alluvium (Qal), found in stream channels, alluvial fans (Qaf), landslides (Qls), and debris flows (Qdf). There is colluvium (Qcl) from hillslopes and another unit, Qc, where a known bedrock ridge exists, but it is covered in a thin layer of colluvium so there are no visible bedrock outcrops. QTg, a gravel deposit overlying several bedrock ridges has an unknown depositional history.

Four inset terrace deposits (Qt1-Qt4) are found alongside stream channels. Most of the creeks in the mapped area only show evidence for the older three fluvial terraces. The only known terrace age from radiocarbon dating is Qt3 (~3 kyr) (Boyle et al., 2023). Parallel to many

of these terraces are glacial deposits showing clear distinctions between the two major glaciations. Lateral and recessional moraines with scattered boulders up to 1.5 m in diameter are associated with younger (~16 kyr) Pinedale moraines (Qpt). Subdued moraines with few boulders reaching 1m in diameter are associated with older (~140 kyr) Bull Lake moraines (Qbt). Reworked Pinedale outwash (Qpo) and Bull Lake outwash (Qbo) are found towards the valley, in front of their respective moraines.

Three main lithologic units underlie the mapped area of the upper Wood River Valley. The Eocene Challis Volcanic Group includes dacite, andesite, and rhyolite tuffs, and the Eocene Challis intrusive rocks are defined by granodiorite and quartz monzonite (Lewis et al., 2012). There is also the Permian and Pennsylvanian sedimentary lithologies of the Wood River Formation, consisting of mostly siliciclastic rocks (Link et al., 1995; Lewis et al., 2012). For purposes of the surficial map, these three bedrock formations have been combined into one undivided bedrock unit on the map.

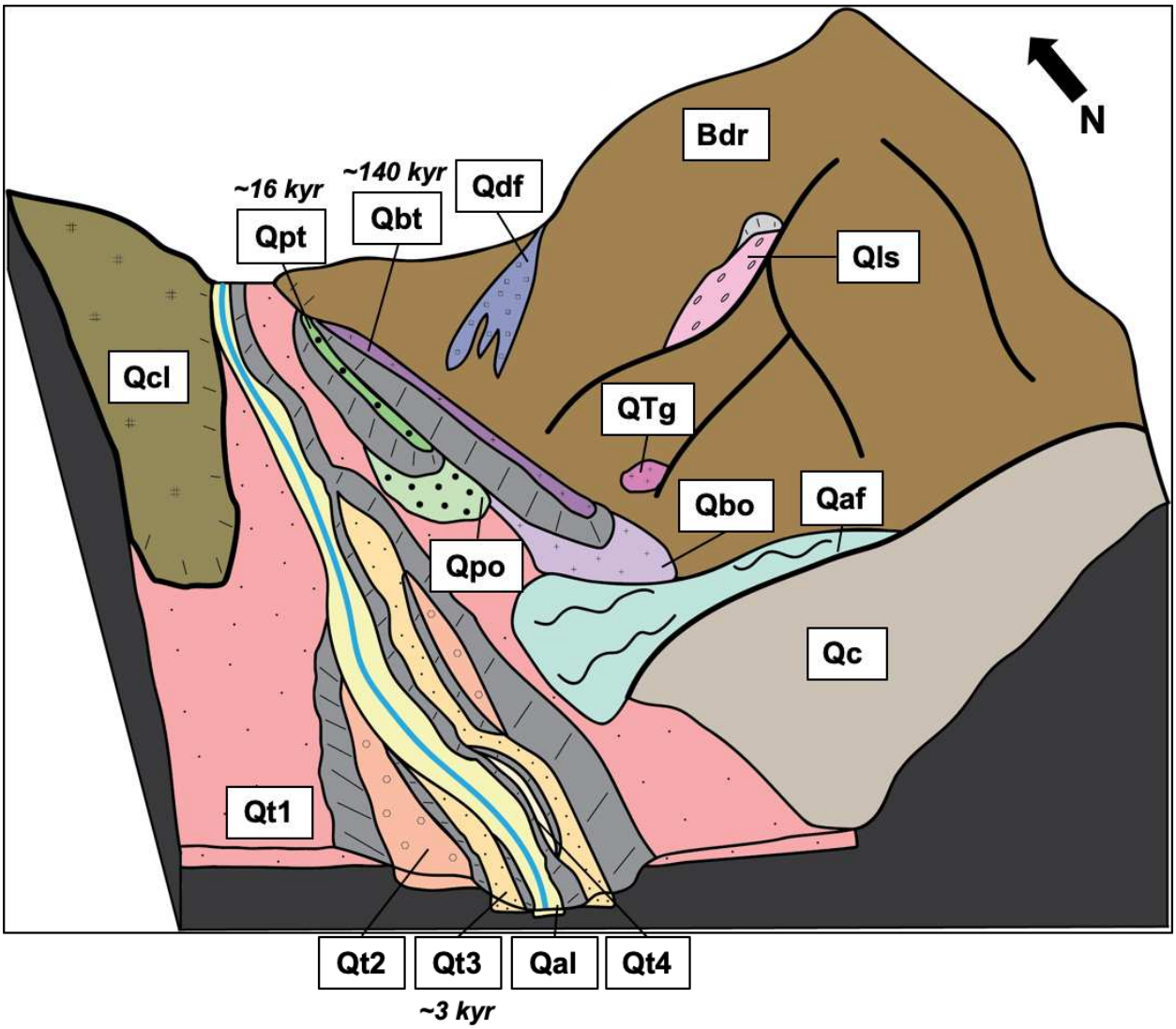

Figure 3. Block diagram of the stratigraphic relationship between surficial units in the Easley Hot Springs and Amber Lakes 7.5' Quadrangles with approximate landform ages. Descriptions of each unit are provided in Appendix A.

3.2. *Fault Segmentation*

Seven distinct segments forming three fault sections spanning over 20 km along strike are observable along the mountain front either in the field or on LiDAR with the likelihood that individual surface fault segments may link at depth (Figure 4). These are apparent segments based on visible breaks in their surface expression. Notably, segments 1 and 2 are separated by a 7.5 km-long reach of no visible scarps. In most segments, the fault scarp is cutting through both

bedrock and alluvial surficial deposits. Segment 5 and segment 6, the longest segment that includes Boulder Creek, also cut through glacial deposits in their respective drainages. Segments 2-5 are close in proximity to one another in the central mapping area with less than ~300 m separating their visible scarps. A distance of 2.3 km separates segments 5 and 6. At the eastern end of the fault, segments 6 and 7 are located relatively close to one another (~170m). The fault dips mainly towards the SW, with sections of some segments dipping to the SE and the segment near Galena Summit, dipping south (Table 1). Also accompanying these divisions are notable changes in the strike orientation. Segment 1 has a western strike orientation. Segments 2-5 produce a concave curve around the range front shifting strike direction from NW to NE. Segments 6 and 7 have a NW strike orientation and are situated much closer to the valley floor.

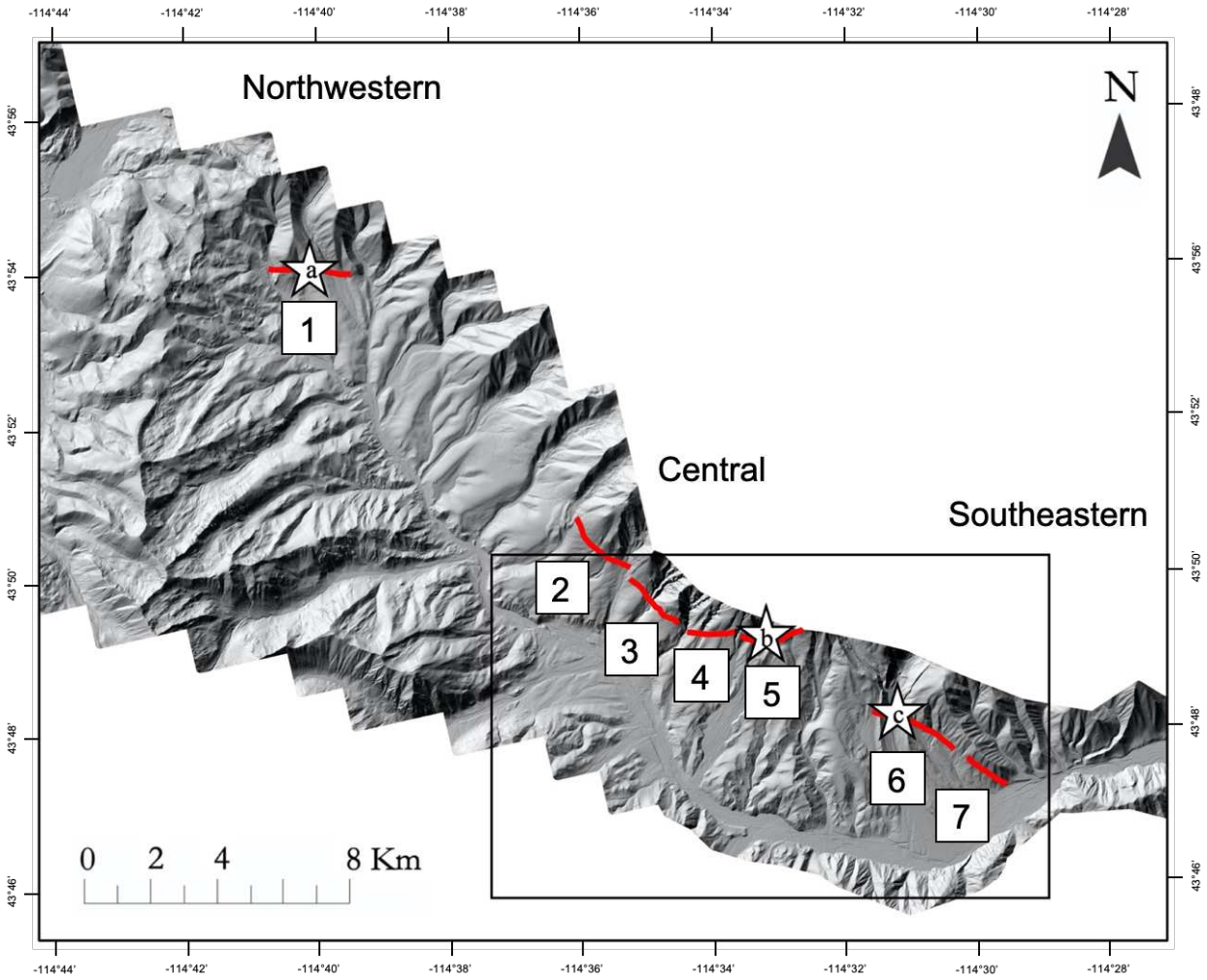

Figure 4. Regional LiDAR image of the 7 Boulder Front Fault segments with soil pit locations where radiocarbon samples were collected. Fault sections (Northwestern, Central and Southeastern) are shown. The black box marks the mapped area (Idaho LiDAR Consortium, 2021).

Table 1. Segment Properties of the Boulder Front Fault

Segment	Length (m)	Strike Orientation Range	Gap Between Previous NW Segment (m) Surface Expression
Segment 1 (Horse Creek)	1949	241˚-305˚	N/A
Segment 2	1079	298˚-346˚	7565
Segment 3	1424	301˚-339˚	198
Segment 4	1009	261˚-289˚	302

Segment 5 (Silver Creek)	1346	220˚-308˚	110
Segment 6 (Boulder Creek)	2227	258˚-340˚	2337
Segment 7	1063	283˚-342˚	173

3.2.1. *Radiocarbon Sampling*

During the 2023 and 2024 field seasons, six radiocarbon samples were collected from hand dug soil pits, 50 cm-130 cm deep, in deposits cut by the fault in three separate drainages (Figure 4). Samples a1, a2 and a3 were collected at segment 1 (Horse Creek), closest to Galena Summit at the western end of the interpreted fault and sample b was collected at the adjacent segment to the NW of Boulder Creek, segment 5 (Silver Creek) (Figure 4; Figure 5). Sample c1 and c2, were collected in 2021 near Boulder Creek at segment 6 (Figure 4; Figure 5). Radiocarbon analysis was conducted at Beta Analytic Testing Laboratory in Miami, Florida to calculate ages and associated errors (Table 2; Appendix B). The radiocarbon samples were all deposited in the youngest footwall block prior to the surface being cut by the fault and were used to determine the maximum age of the most recent rupture at each of the segments. The results of samples a1-a3, on the most western segment of fault, ranged from ~1,100-4,500yr. Sample b yielded results of ~2,200yr. Sample c1 and c2 by Boulder Creek, the main study area, were ~2,800-3,400yr. The multiple samples at sites a and c were in correct stratigraphic order so the younger age represents the maximum rupture timing.

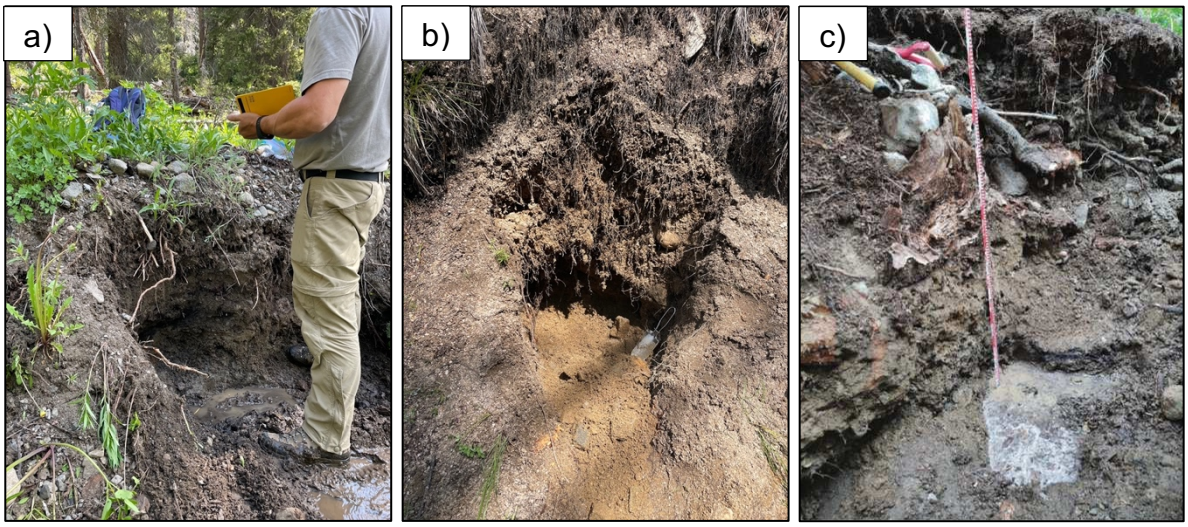

Figure 5. Field photographs of the soil pits where charcoal was collected. Samples were found in the youngest deposit offset by the fault near a) Horse Creek, b) Silver Creek and c) Boulder Creek.

Table 2. Radiocarbon Age Results (Appendix B)

Location	Radiocarbon Age
a1) Horse Creek	1117±63yr
a2) Horse Creek	4475±58yr
a3) Horse Creek	1117±63yr
b) Silver Creek	2206±107yr
c1) Boulder Creek	2813±55yr
c2) Boulder Creek	3410±46yr

3.3. *Fault Scarp Diffusion Modeling*

Ground-rupturing earthquakes produce fault scarps, visible offsets in the topography exposed at the surface. These scarps persist in the landscape for thousands of years, but over time their morphology evolves as they degrade back into the regional slope of the landscape. This occurs by gravitational processes until the angle of repose is reached. Their present-day topographic expression can be modeled by diffusion to estimate the initiation age of the scarp.

Two types of diffusion modeling are presented in this study, a traditional single slip model that requires the user to approximate both the lower and upper slopes of the scarp and a continuous slip model that only requires the upper scarp slope to be reconstructed. Modeling scarps by diffusion is one method of determining the rupture history of faults.

3.3.1. *GNSS Profiling*

Diffusion modeling requires a dataset of distance and elevation across the scarp to model the change in the scarp over time. A Trimble differential GNSS RTK system composed of a base station (Trimble R9s with Zephir 3 antenna) and a rover (Trimble R8s receiver) were used to collect profiles across the scarp in the field and to provide a series of northing and easting coordinates in addition to elevation data. The base station remained in an unobstructed location on the Qt1 surface and a 100 meter tape measure was laid out perpendicular to the scarp. Vertical and horizontal measurements have resolution of 2.5 cm and were taken by the receiver every 2 meters on the footwall and hanging wall blocks and every 1 meter on the scarp. During preliminary fieldwork in 2021, six profiles were measured across the visible fault scarp with an additional profile being measured in 2023 (Figure 6).

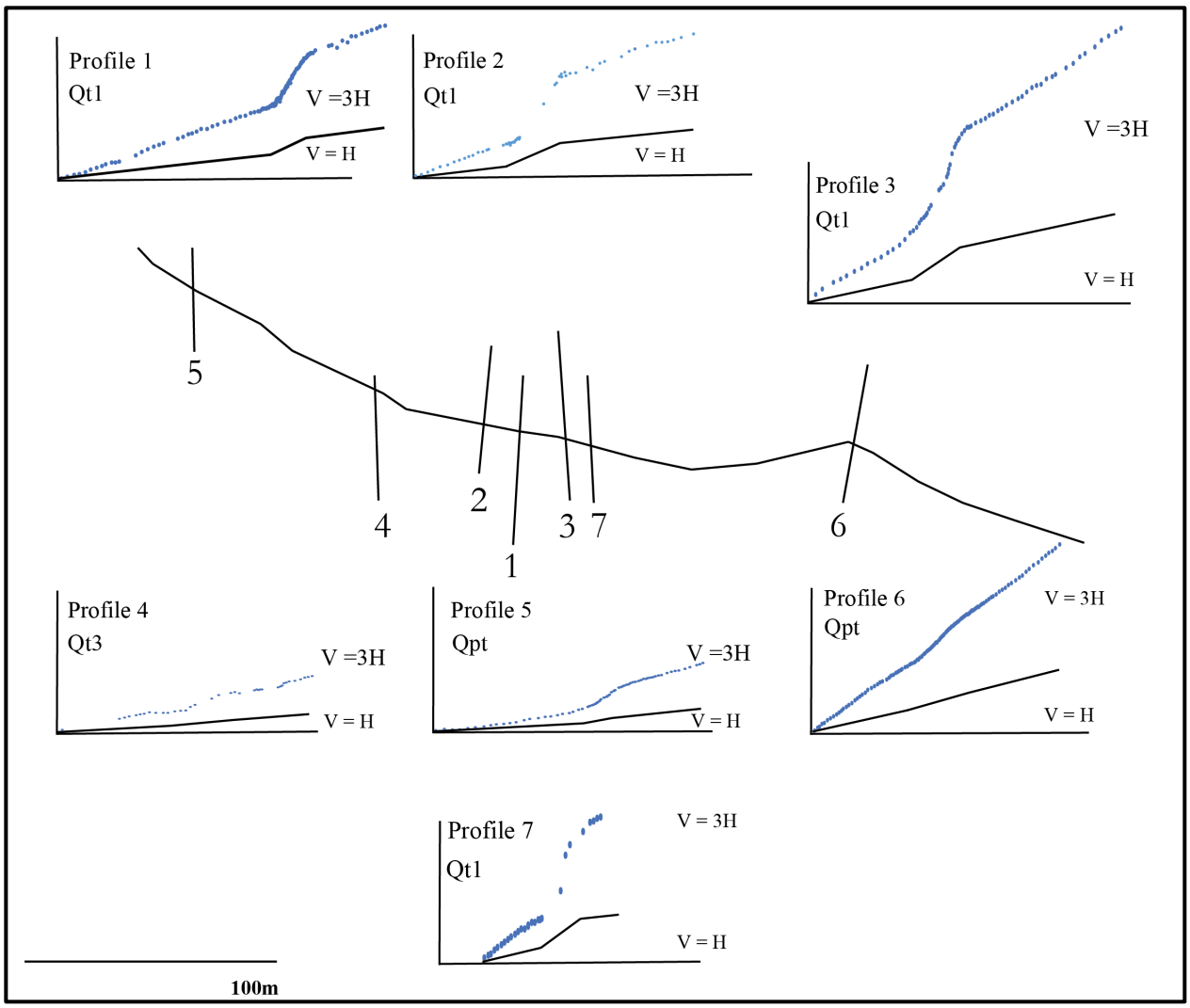

Figure 6. GNSS survey data of the seven profiles with actual elevation (black line) and vertical exaggeration of three times the height (blue dots) collected on the Boulder Creek fault segment. Due to tree cover blocking the satellite signal, profile 4 did not extend far into the fault footwall.

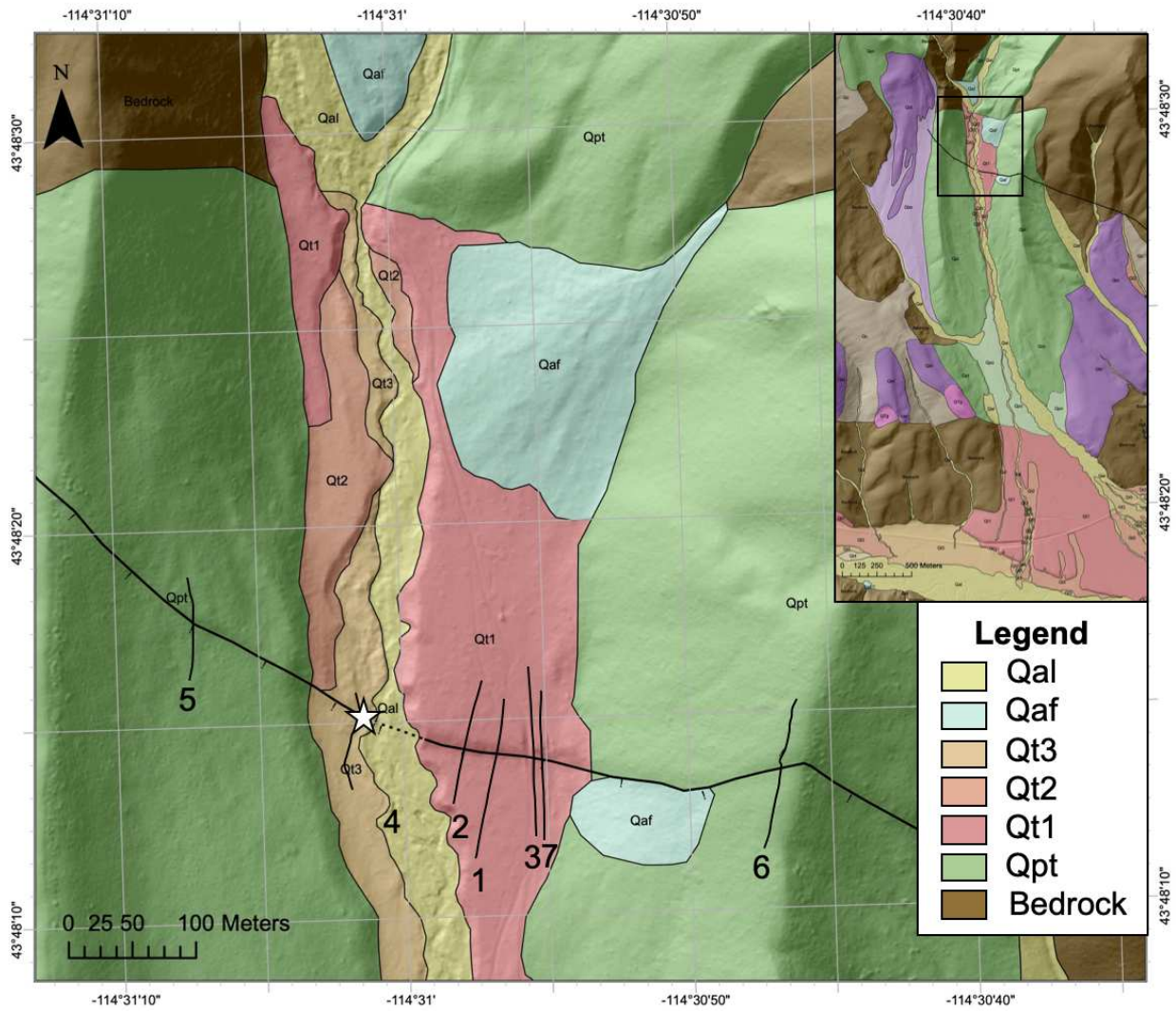

Figure 7. Geologic map of Bull Lake and Pinedale-age glacial deposits along Boulder Creek with the locations of collected profiles and soil pit (white star). Insets show the stratigraphy and the relationship between glacial surface deposits of the Boulder Creek area and Big Wood River deposits.

Profiles 1-3 and 7 were collected in the oldest river terrace deposit, Qt1, and profile 4 was located in the younger inset terrace deposit, Qt3. Profiles 5-6 were measured in the bounding parallel Pinedale lateral moraines, Qpt (Figure 7). Due to anthropogenic effects from nearby construction on the road leading to the abandoned mining village of Boulder City, profile 3 was not used for timing and slip rate determination during data analysis and interpretation. During the

2023 field season, profile 7 was measured directly east of profile 3 to ensure accurate measurements with no anthropogenic effects.

3.3.2. *Diffusion Coefficient*

A linear diffusion equation can be used to model the fault scarp ages (Hanks, 2000; Regalla et al., 2007). In this equation, the observed scarp slope (du/dx), half offset between the hanging wall and footwall (a), and regional slope (b), are measured from the profile. An initial scarp slope (α) correlating to the angle of repose is set at 35°. Time (T) in kyr is the rupture age variable being solved by fault scarp diffusion modeling discussed below. K is the diffusion coefficient in m^2/kyr and erf is the error function.

$$\frac{\mathrm{d}u}{\mathrm{d}x}\Big|_{x=0} - b = (\alpha - b)\,\mathrm{erf}\left[\frac{(a/(\alpha - b))}{2\sqrt{(KT)}}\right] \quad (1)$$

Diffusivity of material on a fault scarp is aspect-dependent due to north-facing and south-facing slopes have differing microclimates (Pierce & Colman, 1986). These differences include solar radiation, vegetation that stabilizes soils, wind, and soil wash. The Boulder Front fault is a SW-facing scarp. Diffusion coefficients are also heavily dependent on the height and steepness of the scarp (Pierce & Colman, 1986). Given that all profiles were collected in close proximity on the same fault segment, microclimate was unlikely to vary on the GNSS profiles collected.

A range of published diffusion coefficients in the Northern Basin and Range Province for scarps of similar heights, between 5-10 m, ranges from 0.98-3.4 x10^{-3} m^2/kyr (Pierce & Colman, 1986). A diffusion coefficient of 1.26 x10^{-3} m^2/kyr was previously determined from studies in the unconsolidated fluvial sediment in the eastern Red Rock Valley, 186 km to the NE, however,

these unconsolidated surficial deposits were from alluvial fans in a drier climate (Harkins et al., 2005; Regalla et al., 2007).

Using the known maximum rupture age from the soil pit near profile 4 (~2.81kyr) and the modeled *KT* value of the profile, a *K* of 2.09×10^{-3} m^2/kyr was calculated for the region where the Boulder Front fault is located. This value falls close to the published values of both Regalla et al., (2007) and Pierce and Colman, (1986). Diffusion calculations using both the Regalla et al. (2007) published value and the locally calibrated diffusion coefficient are modeled.

3.3.3. *Single Slip Modeling*

Scarps decay by gravitational processes once formed, until reaching an angle of repose, which is assumed by the model to be 35°. Diffusion then occurs until the surface offset is removed and the scarp reaches the same angle as the regional slope (Figure 8). The regional slope was determined directly from GNSS profiles (Appendix C). Initial fault ages are calculated based on the time between the scarp at the angle of repose after initial ground rupture and the slope of the currently modeled profile.

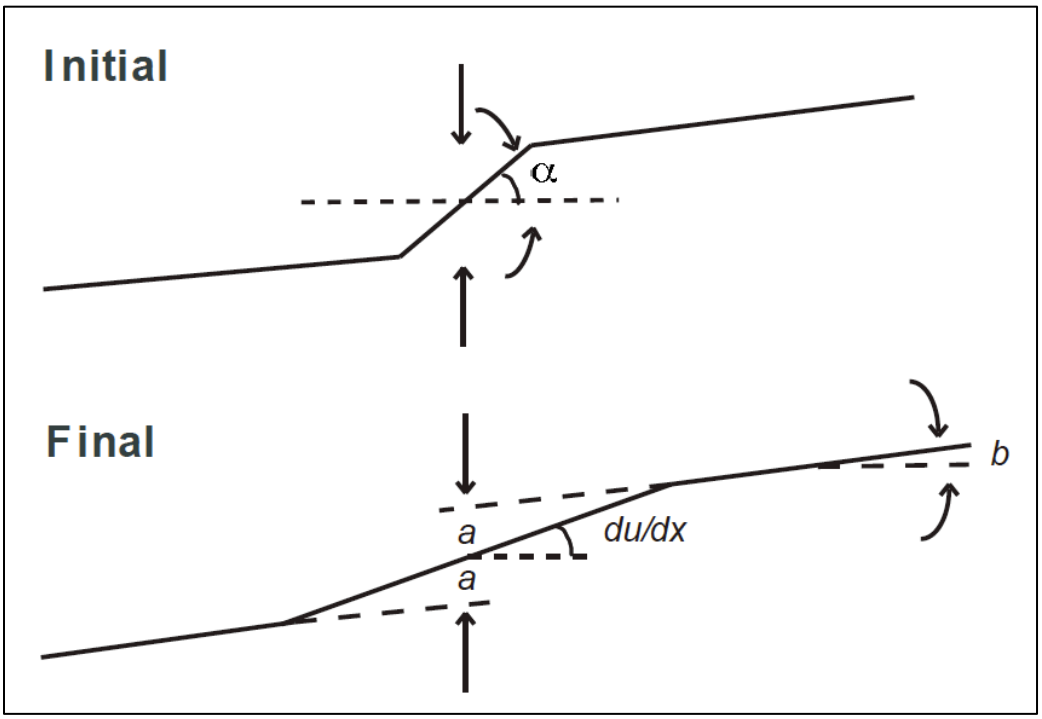

Figure 8. The process of fault scarp degradation over time (from Regalla et al., 2007).

The distance and elevation GNSS profile data is imported into MATLAB R2022a-R2024a for use in a single slip diffusion code that assumes only one ground rupturing earthquake occurred to create the scarp (Appendix D). MATLAB prompts the selection of the fault midpoint, upper regression, and lower regression of the regional slope for each profile (Nash, 2005; Regalla et al., 2007). The output of the code produces a simulation of the scarp degrading over time and an estimated rupture age (T) of the fault using the chosen diffusion coefficient (Appendix D). The average rupture age of each profile is then input into a Monte Carlo simulation to express uncertainties on the scarp height and regional slope in the single slip code (Regalla, personal communication, 2022; Appendix E). The limitations of the single slip model are the assumption of only one event producing the scarp and the use of the lower scarp slope that is prone to sediment accumulation which may shallow the slope.

3.3.4. *Continuous Slip Modeling*

There is evidence of multiple ground rupturing earthquakes on the Boulder Front fault based on mapping and scarp height, in various surficial deposits. The continuous slip rate method is used when the rupture history of multiple events is not known for a fault as is the case for the Boulder Front fault (Figure 9). The model assumes a constant slip rate occurring by means of small vertical displacement (<1mm) which degrades the scarp by diffusion (e.g., Mattson & Bruhn, 2001). The continuous slip model only uses the upper background slope as opposed to the single slip model which uses both the upper and lower slopes. The accumulation of material from lateral sediment transport and wind is the reason for excluding the lower slope (Mattson & Bruhn, 2001).

The continuous slip code prompts users to enter a far-field slope (*b*), the same as the regional slope in the single slip model, half-surface offset (*a*), diffusion constant (*K*). It also requires a series of three half-slip rates (*A*), a minimum and maximum age (*t*), and a time step. Elevation (*u*) and horizontal distance (*x*) are accounted for by the profiles. Erf is the error function and sgn is a sign function. The output is an overlay of an observed profile and best-fit model. It also provides a *KT* value which can be divided by the input *K* to determine initial the rupture age of the profile. Variable half offset was used by modeling an offset of 0.1m both higher and lower than the best-fit data to provide errors on the rupture age.

(2)
$$u(x,t) = (a + At)\operatorname{erf}\left(\frac{x}{2\sqrt{\kappa t}}\right) + \frac{Ax^2}{2\kappa}\left[\operatorname{erf}\left(\frac{x}{2\sqrt{\kappa t}}\right) - \operatorname{sgn}(x)\right] + \frac{Ax}{\kappa}\sqrt{\frac{\kappa t}{\pi}}e^{\left(-x^2/4\kappa t\right)} + bx .$$

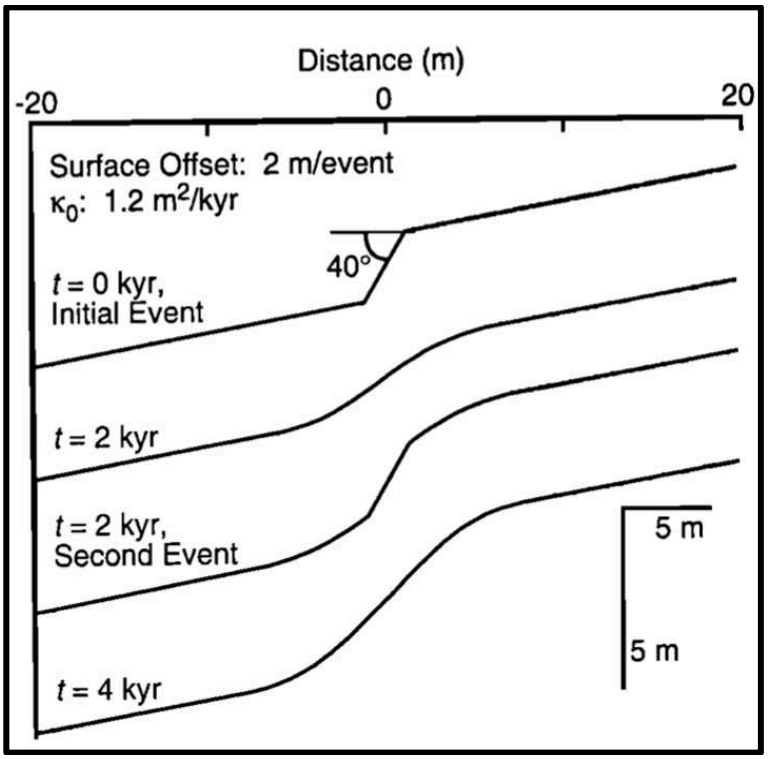

Figure 9. The change in a fault scarp profile after two surface-rupturing events (from Mattson and Bruhn, 2001).

3.3.5. *Rupture Age*

Used in combination, these models likely bracket the fault initiation age. Single slip diffusion models provide an estimate of the maximum rupture age of the fault assuming the slip is all linked to one large rupture event. In contrast, the continuous slip diffusion model provides an estimate of the minimum rupture age of the fault. The rupture age is very dependent on the diffusion coefficient (*K*). Using the closest Regalla et al., (2007) published diffusion coefficient (1.26×10^{-3} m^2/yr), single slip modeling estimates a maximum rupture age of 7.08kyr±0.68kyr while continuous slip modeling estimates a minimum age of 4.96kyr±0.41kyr for the Boulder Creek fault segment (Figure 10a). Using a locally calibrated diffusion coefficient (2.09×10^{-3} m^2/yr), single slip modeling estimates a younger maximum age of 4.27kyr±0.68kyr while continuous slip modeling estimates a minimum age of 2.99kyr±0.41kyr (Figure 10b).

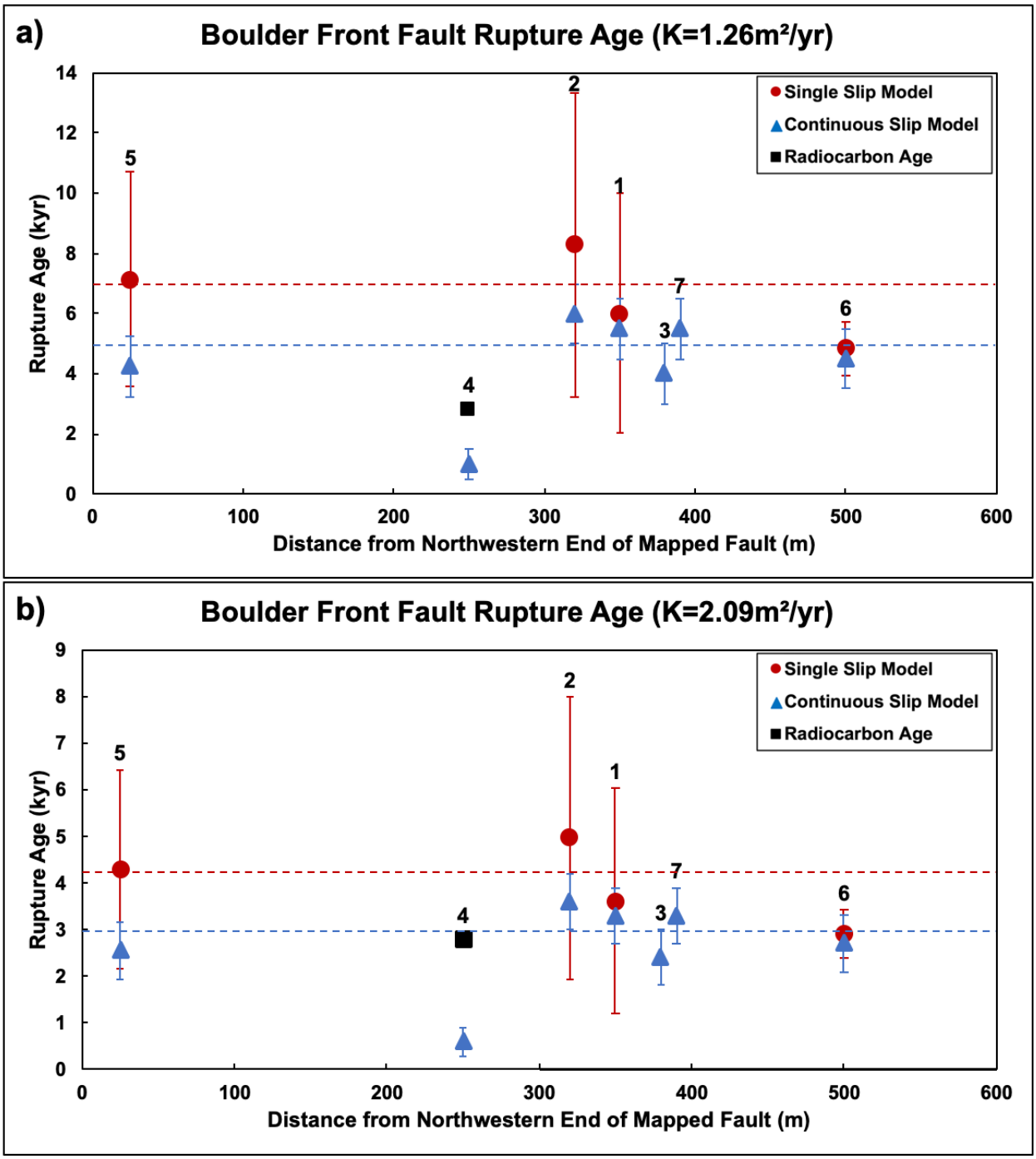

Figure 10. Rupture ages of the fault for both single slip and continuous slip diffusion modeling and the radiocarbon dated charcoal sample using diffusion coefficients a) $K=1.26x10^{-3}$ m^2/yr b) $K=2.09x10^{-3}m^2/yr$. Circles and triangles represent the single slip and continuous slip modeling results respectively. The square is the radiocarbon age from the soil pit near profile 4 marking the maximum of the most recent rupture. Dashed lines correspond to the weighted averages of each model.

3.3.6. *Amount of Slip*

The amount of slip is measured as the vertical difference in height between the offset regional slopes of the fault based on the measured fault profiles. The average amount of slip on the Boulder Front fault on the older Qpt and Qt1 deposits (Profiles 1-3, 5-7) is 4.94 m (Figure 11). Based on the measured offset from profile 4, in the youngest terrace, there was only 0.74m of slip on the Qt3 deposit. Profile 4 was not included in the overall average amount of slip.

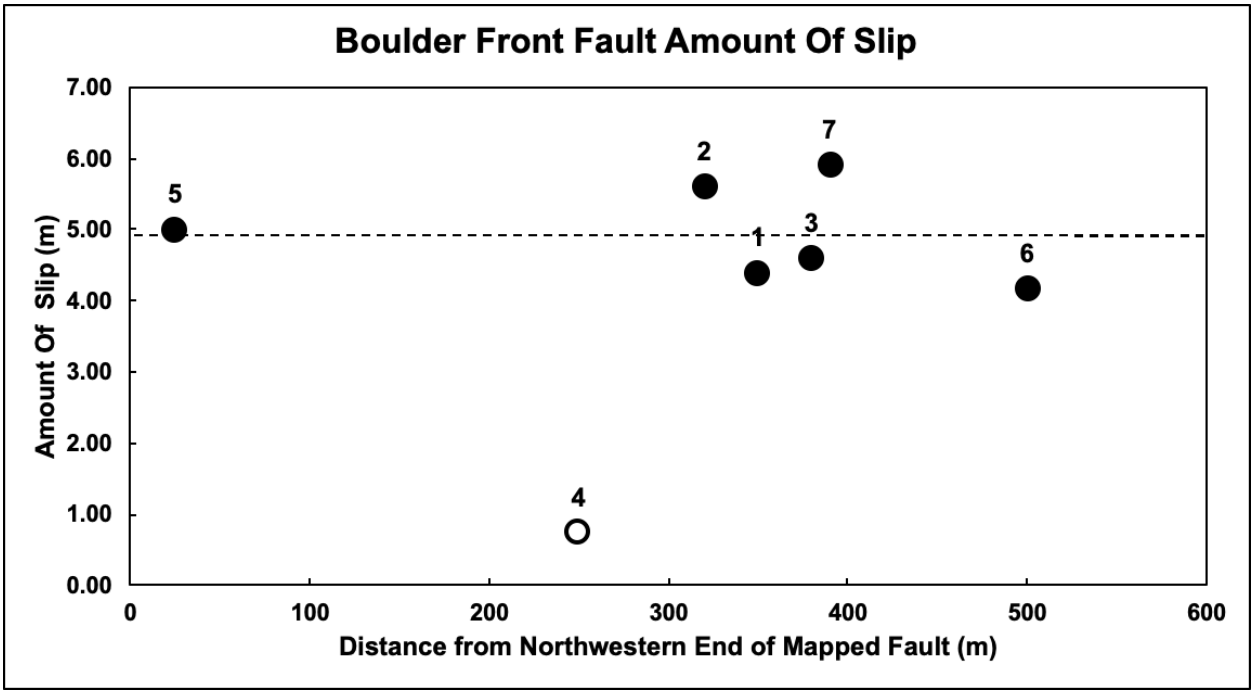

Figure 11. The amount of offset on the Boulder Creek segment. Profile 4, the open circle, is in an inset deposit and therefore is less offset. Only the closed circles, marking older deposits, are included in the average. The dashed line represents the average of 4.94m.

3.3.7. *Slip Rate*

The youngest sample from the soil pit near profile 4 produced an age of ~2.81 kyr (Table 2). This age was used along with the height of the scarp in the Qt3 deposit from the field (~0.52 m) to calculate the slip rate at that section of the scarp segment (Figure 12). An estimate for the age of the lateral moraines is calculated by averaging the terrestrial cosmogenic nuclide (TCN) ages of recessional moraines located ~50 km NW of the Boulder Front fault near Redfish Lake

(Easterbrook et al., 2011). Results showed the last glaciation event to have ended ~15.76kyr. These dates were used in conjunction with the amount of slip on profiles 5 and 6, also on the Pinedale moraines, to calculate the slip rate of the Boulder Creek segment in the Qpt surface. Using these age estimates, the average slip rate across profiles 4-6 is ~0.26mm/yr (Figure 12).

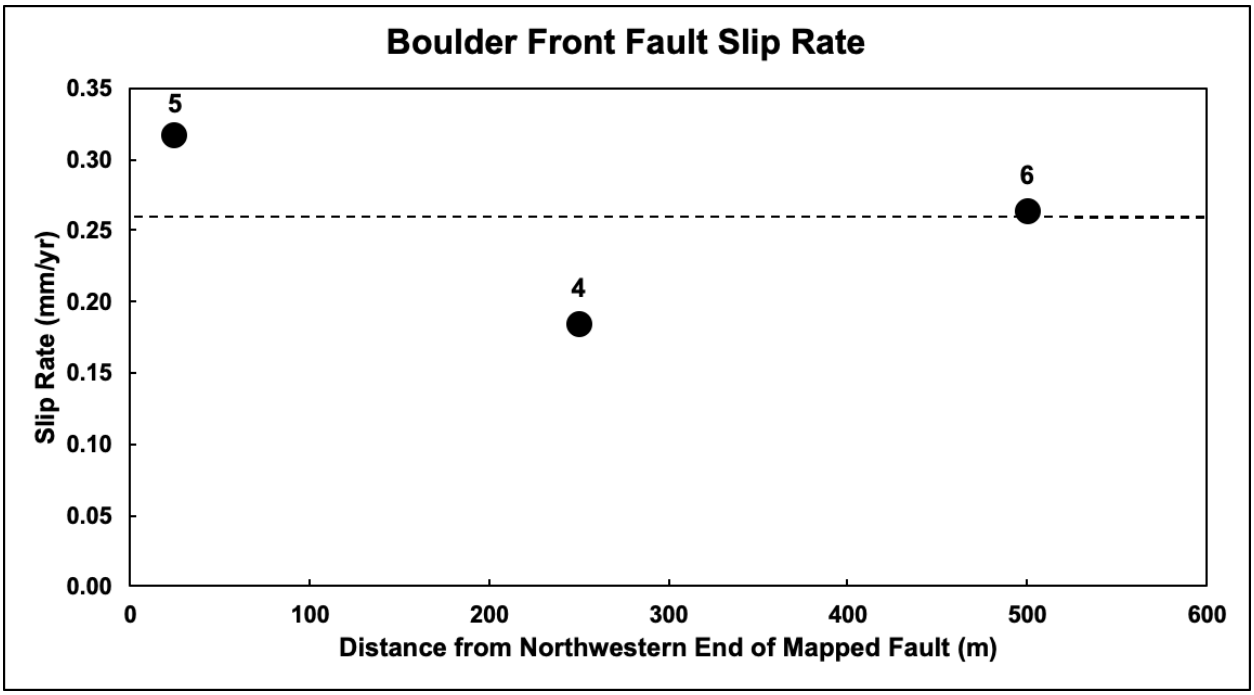

Figure 12. The average slip rate for the Boulder Front fault using profiles 4-6. The dashed line represents the average of 0.26mm/yr.

4. Regional Erosion and Uplift Methods and Results

4.1. *Field Methods*

The study thus far has been focused on the area SE of Galena Summit in the upper Wood River Valley. A regional erosion and uplift rate study was conducted across both the upper Wood River Valley and adjacent Sawtooth Valley, north of Galena Summit. The experiment involved the collection of samples of quartz-rich sand in seven catchments for the determination of Beryllium-10 (^{10}Be) concentrations, erosion rates, and modeled uplift rates throughout the region

on both sides of the axial drainages, in both the hanging wall and footwall blocks and where the land surface was and was not ruptured by a fault (Figure 13).

On the west side of the valley, one sample was collected in the northern aftershock region of the 2020 Stanley earthquake in the Lola Creek catchment on Cape Horn Mountain. Two samples were collected on the west side of the Sawtooth Valley along the Sawtooth fault in the Crooked Creek and Huckleberry Creek catchments. Another was collected on the opposing side of the valley from the Sawtooth fault in the Gold Creek catchment. A sample on the east side of Galena Summit was collected in the Senate Creek catchment. Samples were collected on opposite sides of the upper Wood River Valley, in the Boulder Creek catchment, offset by the Boulder Front fault, and the Logged Canyon catchment (Figure 13). Another sample was in the Eagle Creek catchment, south of the fault and nearest to Sun Valley and Ketchum, Idaho, however, not enough quartz was found for analysis in the sample, so it was unable to be used in data interpretation.

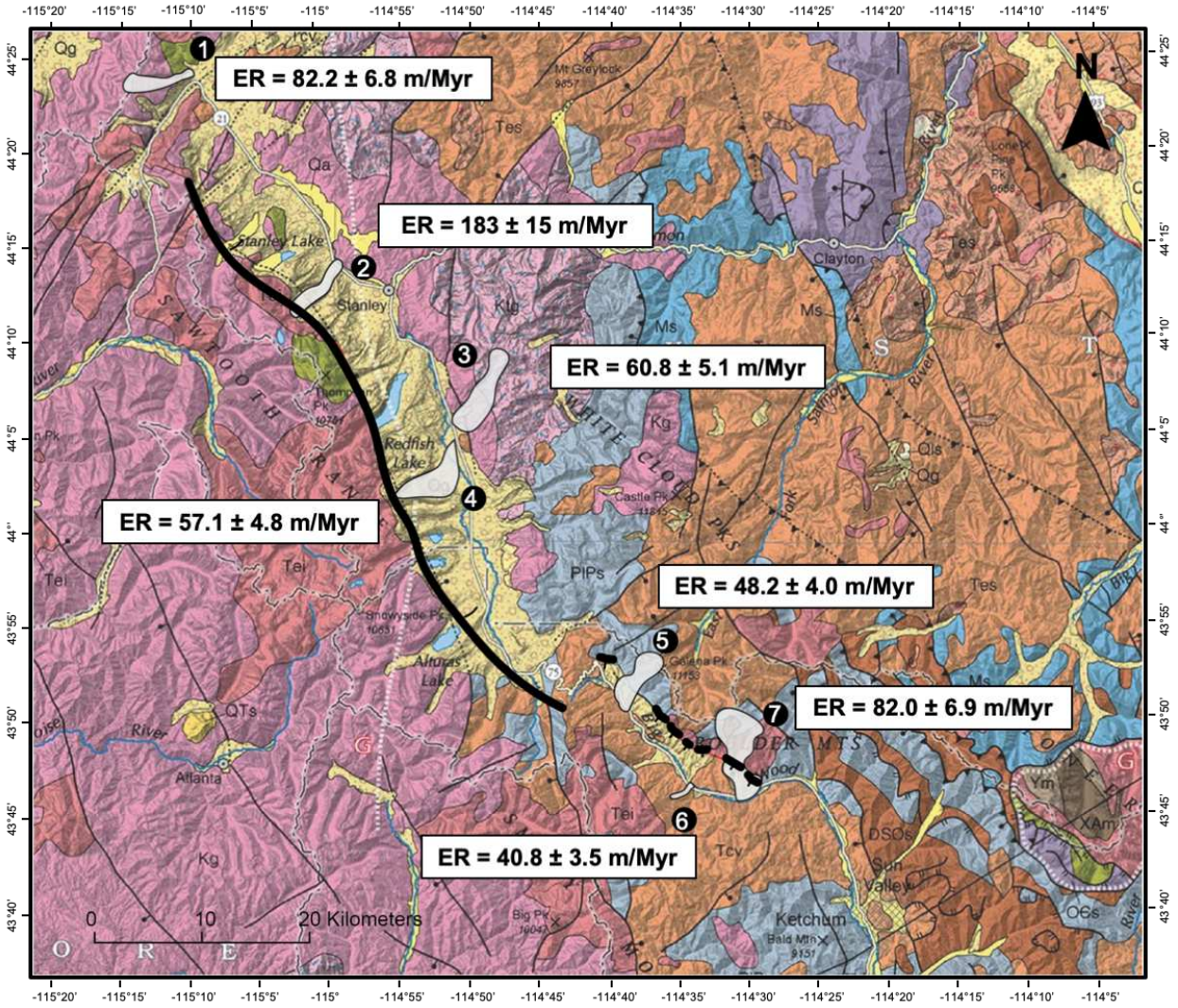

Figure 13. Map of the catchments sampled and corresponding erosion rates (ER) with errors in the Wood River and Sawtooth valleys. Catchments: 1) Lola Creek, 2) Crooked Creek, 3) Gold Creek, 4) Huckleberry Creek, 5) Senate Creek, 6) Logged Canyon, 7) Boulder Creek. Geologic base map modified after Lewis et al., 2012.

The field methodology involved collecting ~1-2 kg of sand near the mouth of the catchment, to integrate erosion rates across the entire drainage, and sieving the samples to less than 2mm. The sediment was sieved to account for soil-mantled hillslopes (Belmont et al., 2007). Sediments finer than 0.25mm may have been windblown from nearby catchments and therefore are not included in the study (Granger et al., 1996).

4.2 Lab Analysis

To determine erosion rates, initial sample preparation included sieving samples between 0.25-2 mm, washing with water to remove fines, and HCl dissolution of carbonates at Lehigh University facilities. The samples were sent to the Wollongong Isotope Geochronology Laboratory in Australia for quartz separation and purification, chemical preparation (BeO), and Accelerated Mass Spectrometry measurement for [^{10}Be]. The results from the laboratory analysis are presented in Table 3.

4.3. *Erosion Rates*

Table 3. Accelerated Mass Spectrometry Results

Catchment	[^{10}Be] atoms/g	[^{10}Be] Uncertainty atoms/g
1 (Lola Creek)	1.406E+05	3.328E+03
2 (Crooked Creek)	6.451E+04	1.601E+03
3 (Gold Creek)	2.043E+05	5.217E+03
4 (Huckleberry Creek)	2.173E+05	5.139E+03
5 (Senate Creek)	2.899E+05	7.404E+03
6 (Logged Canyon)	3.103E+05	9.703E+03
7 (Boulder Creek)	1.459E+05	3.804E+03

Results from the AMS analysis produced nuclide concentrations with associated uncertainties for each sample (Table 3). Erosion rates were calculated through the CRONUS-Earth online erosion rate calculator (Balco et al., 2008). The program requires inputs from both the field and the lab to be entered in a specific input layout for erosion rate calculation (Appendix F). Topographic shielding is the last input and can be calculated for remotely to accurately solve for erosion rates. 90 m DEM's and hydrography data downloaded from the USGS National Map Data are imported to ArcGIS Pro. The raster can be converted to a .txt file

using the Raster to ASCII tool. The .txt file is read into a MATLAB script designed for the analysis of catchments and long profiles that involve MATLAB functions from TopoToolbox (Schwanghart & Scherler, 2014; Pazzaglia, personal communication, 2024). In the code, the studied drainage basin can be selected and its topographic shielding calculated. The MATLAB script will not produce a number for topographic shielding and therefore the newly generated file must be exported to ArcGIS Pro as a .geotiff file. Viewing statistics of the watershed, and subtracting the mean value from 1, will indicate the topographic shielding correction for that watershed. The shielding values ranged from 0.948 to 0.993 (Appendix F).

All erosion rate results except one range by a factor of two from 40.8±3.5m/Myr to 82.2±6.8m/Myr (Table 4). The outlier is sample 2, Crooked Creek catchment, with an erosion rate of 183±15 m/Myr. The integration time for [^{10}Be] to represent a basin wide erosion rate is inversely proportional to the erosion rate. For slowly eroding landscapes, the integration time is long, on the order of 10^4-10^5 years. In contrast, for rapidly eroding landscapes, the integration time is short, on the order of 10^3-10^4 years. For the [^{10}Be] and erosion rates presented here, the integration time is on the order of 10^4 years, spanning at least the glacial cycle.

Table 4. Regional Catchment Properties

Sample	Erosion Rate (m/Myr)	Drainage Basin Area (km^2)	Fault Scarp Present
1 (Lola Creek)	82.2 ± 6.8	6.950	No
2 (Crooked Creek)	183 ± 15	15.885	Yes
3 (Gold Creek)	60.8 ± 5.1	35.142	No
4 (Huckleberry Creek)	57.1 ± 4.8	17.139	No
5 (Senate Creek)	48.2 ± 4.0	6.560	No
6 (Logged Canyon)	40.8 ± 3.5	0.896	No

7 (Boulder Creek)	82.0 ± 6.9	18.605	Yes

4.4. *Catchment-Scale Uplift Modeling*

The linear inversion of the longitudinal river profiles is a modeling methodology used to reconstruct base-level fall histories corresponding to uplift rates of individual catchments (Fisher et al., 2022). The code, available in Fisher et al., 2022, uses digital elevation models of watersheds to model the fluvial topography (Figure 14). The initial inputs to the model are a 90 m clipped DEM of a watershed, ^{10}Be erosion rate with the associated error, a concavity value and critical drainage basin area. The model, based on a series of stream-power equations, calculates the normalized steepness for each basin by using the concavity value, set at the global average of 0.45, for all the catchments (Kirby et al., 2003; Fisher et al., 2022). Erodibility can then be modeled using the normalized steepness index and erosion rate for each catchment. The version of the model being used in this study assumes a uniform geology and therefore a constant erodibility for the bedrock in each of the drainage basins (Goren et al., 2014). One caveat of the model is that all of the samples are from alluvial streams and the model assumes they are bedrock streams. The inversion of the longitudinal profiles is used to determine the-base level fall history which is assumed to equate to spatially uniform uplift rates across each of the individual catchments. A timestep of 0.25 Myr was used to account for multiple glacial-interglacial cycles and the Monte Carlo simulation was set for 100 iterations to express uncertainties in the normalized channel steepness, erosion rates and erodibility (Fisher et al., 2022). The results are showing the uplift rates from the modeled base-level fall history from each catchment's respective erosion rates, steepness and erodibility (Figure 15).

Modern modeled uplift rates of the catchments range from 0.01mm/yr to 0.08mm/yr (Figure 15). The lowest is Senate Creek catchment with a rate of 0.01 mm/yr and then Gold Creek, Huckleberry Creek, and Logged Canyon catchments with uplift rates of 0.02 mm/yr. Yielding higher present-day uplift rates are Lola Creek catchment, 0.05 mm/yr, Boulder Creek catchment, 0.07 mm/yr, and Crooked Creek catchment, 0.08 mm/yr. Variability in erosion rates may reflect mass flow deposits abundance upstream of the ^{10}Be sample.

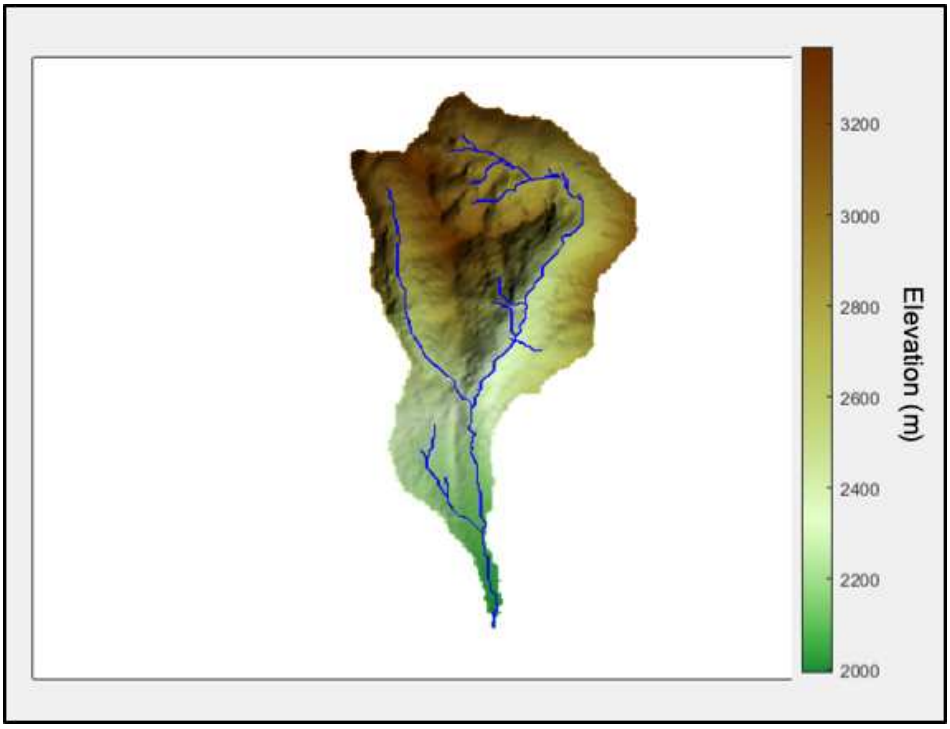

Figure 14. Colored shaded relief map of the Boulder Creek watershed.

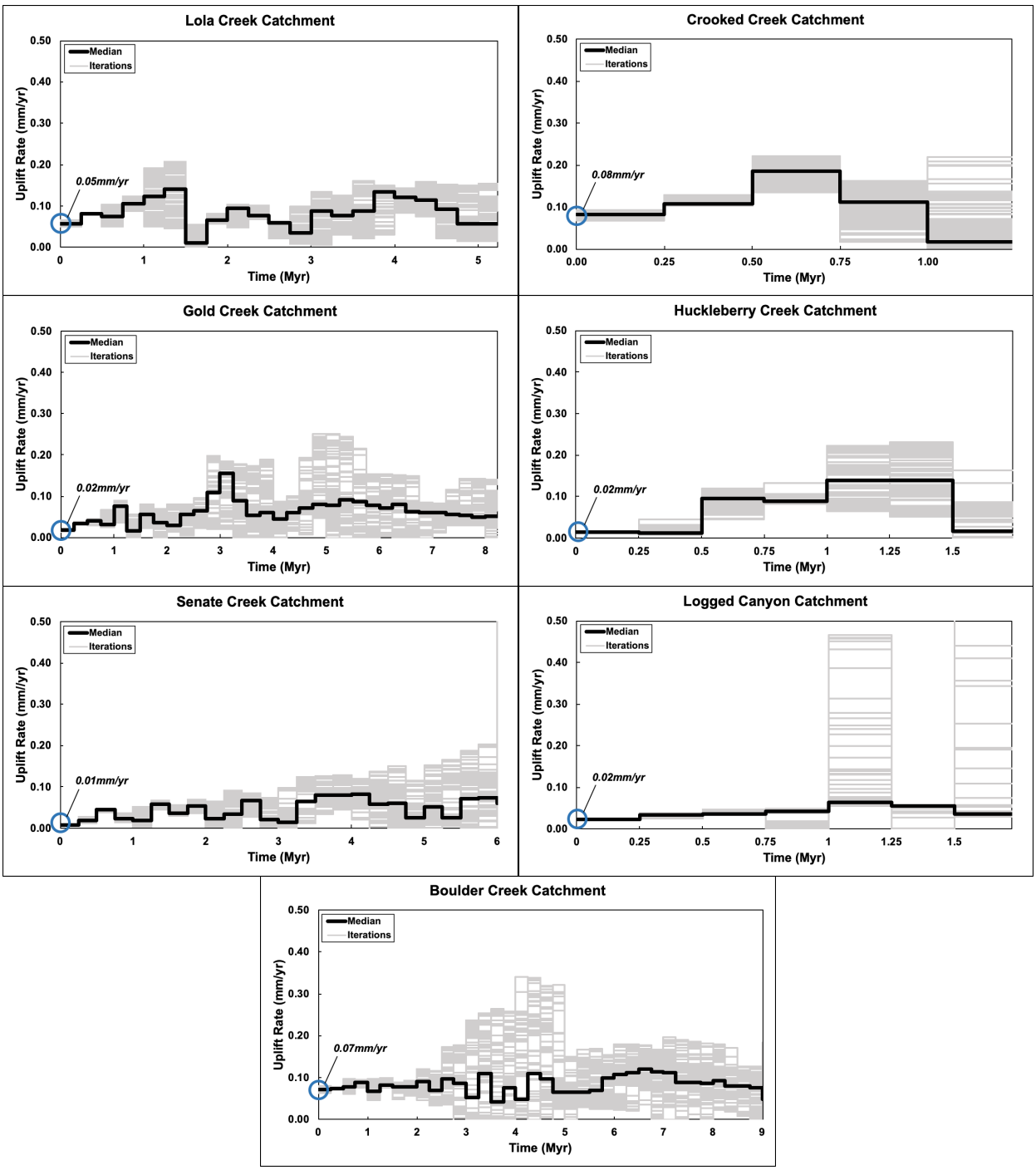

Figure 15. Long-term uplift rates of a) Lola Creek catchment, ER= 82.2±6.8m/Myr, b) Crooked Creek catchment, ER=183±15m/Myr, c) Gold Creek catchment, ER=60.8±5.1m/Myr, d) Huckleberry Creek catchment, ER=57.1±4.8m/Myr, e) Senate Creek catchment, ER=48.2±4.0 m/Myr, f) Logged Canyon catchment, ER=40.8±3.5m/Myr, g) Boulder Creek catchment, ER=82.0±6.9m/Myr. Gray lines are the 100 iterations of the Monte Carlo simulation and the black line is the median of all the runs. Blue circles mark the modeled modern base-level fall/uplift rate.

5. Discussion

5.1. *Fault Characterization*

Interpretation of DEM's and field mapping have extended the mapped length of the Boulder Front fault to Galena Summit while revealing 7 segments spanning over 20 km across the southern face of the Boulder Mountains. The average segment length of a normal fault in the Northern Basin and Range has been reported to be 20-25 km, consistent with the length of the entire Boulder Front fault (Jackson & White, 1989; Crone & Haller, 1991). In comparison to other normal faults in the Northern Basin and Range, segments of the Boulder Front fault are considerably shorter, measuring from 1.1 km – 2.2 km. A study on active faulting in the Northern Basin and Range of Montana and Idaho reveals fault segments are generally oriented N30°W to N55°W and N75°W to S80°W (Stickney & Bartholomew, 1987). While most of the strike orientations of the Boulder Front fault segments fall within these values, a few outliers stretch the range from S40°W-N14°W.

Gaps in the continuity of a scarp and changes in its morphology are used to define the characteristics of fault segment boundaries associated with normal faults (Crone & Haller, 1991). This allows for the characterization of the Boulder Front fault into three main sections: northwestern, central, and southeastern. Although the fault scarp is not continuous across the central section, most of the minor gaps between the segments are confined to either bedrock or alluvial and mass movement deposits. Recent erosion and stream channels may be responsible for concealing scarps in Quaternary deposits, however, bedrock being more resistant to weathering should enhance the surface expression of the fault (Hilley et al., 2001). While there is no visible linkage of segments 2-5, the proximity and morphology of the scarps lead to the implication of linkage in the subsurface. The observed lack of continuous fault scarp expression

suggests that the Boulder Front fault is still immature and the accommodation zone is not breached as the fault segments have yet to link up (Cowie, 1998; Harkins et al., 2005).

The radiocarbon dating results corroborate the interpretation of the fault segmentation. The samples near segment 1(Samples a1-a3) are too large of a range to make determinations of its relationship with segment 6 (Sample c1-c2) at Boulder Creek. The young radiocarbon age suggests that segment 1 ruptured within the last ~1,100yrs. The youngest results of samples b and c are much closer (2206±107yr and 2813±55yr) which indicates there could have been a ground rupturing earthquake in approximately the last ~2,200 years as the 14C samples were collected well below (~50-130cm) the ruptured surfaces. Based on scarp morphology and the absence of a continuous surface rupture, (Crone & Haller, 1991), it is unlikely that segments 5 and 6 are linked. Segment 6 at Boulder Creek is also situated much further into the valley than the other segments that are closer to the mountain front.

Seismogenic linkage implications between segments of the Boulder Front fault provide insight into the magnitude of past and future earthquakes. The rupture length of a fault is correlated to the magnitude of the earthquake that occurs (e.g., Wells & Coppersmith, 1994; Wesnousky, 2008). Empirical regression equations comparing surface rupture length to Moment Magnitude (M) estimate the 2.2 km segment at Boulder Creek to have produced an earthquake with M5.5 (e.g., Wells & Coppersmith, 1994). Using the same correlation, had the entire fault ruptured, a length of 20.8 km, it would be consistent with an earthquake with a M6.5. Wells and Coppersmith (1994) have been noted to underestimate earthquake magnitude for larger events (Stirling et al., 2002; Morell et al., 2020). Following instrumental era regressions, the size of the Boulder Creek segment and the entire fault rupture would have been M5.7 and M6.6 respectively (Stirling et al., 2002). It was also noted earlier that earthquakes with <M6.0 may produce poor

surface expression and inconsistencies which implies that the magnitude of the Boulder Creek segment may be at higher than the estimation by Stirling et al., 2002 and at least M6.0 if subsurface linkage is present between the adjacent segments (Wells & Coppersmith, 1994). Although some segment linkage is possible, based on the large distance between the fault sections, it is unlikely that the entire Boulder Front fault ruptured at the same time. However, given the short segment length and the consistency in scarp height it is likely the entire Boulder Creek segment ruptured within the last several millennia.

5.2. *Boulder Front Fault Slip Behavior*

It is evident that there were at least two distinct ruptures of the Boulder Front fault in the last ~7 kyr. An older modeled rupture calculated through diffusional modeling, occurring around 3-7 kyr ago is portrayed in profiles collected in the Qt1 and Qpt deposits. A more recent rupture at the Boulder Creek segment is highlighted by the radiocarbon date of the Qt3 deposit indicating that the latest rupture took place within the last ~<2.81 kyr as the deposit had experienced a surface rupturing earthquake.

Furthermore, the amount of slip on each of the profiles in their respective deposits emphasizes the disparity between the minimal two ruptures at the Boulder Creek segment. An average slip of 4.94m in the older deposits (Qpt and Qt1) is explained by these deposits undergoing more ground-rupturing earthquakes and therefore increasing the amount of slip over time. Less offset, 0.74 m, is apparent in the youngest Qt3 deposit leading to the conclusion that the segment has experienced at least one major rupture prior to Boulder Creek incising to form the inset terrace. The similarities in slip amongst the older deposits also imply that the entire segment ruptured at the same time.

Another method based on the amount of slip would be to assume characteristic earthquakes, when fault segments produce earthquakes of about the same magnitude and displacement (Schwartz & Coppersmith, 1984). A single ground rupturing earthquake on the Boulder Creek segment could produce ~0.7 m of slip and therefore the older deposits experienced ~7 separate events to get a total slip of nearly 5 m. There also could have been fewer events that produced larger amounts of slip. The lateral and recessional moraines consisting of the Qpt deposit are known to be ~15.76 kyr old (Easterbrook et al., 2011). By estimating 7 ruptures since that time, there is a recurrence interval of about 2.3 kyr implying the next earthquake north of Ketchum and Sun Valley, Idaho may be in the near future. These glacial landscapes at the Boulder Creek segment experienced at least 2, but possibly as many as 7 or more earthquakes of M6.0 or greater to produce surface ruptures since their deposition in the late Pleistocene (Easterbrook et al., 2011).

Studies on faults throughout the Northern Basin and Range calculate long-term normal fault slip rates to be 0.2-0.3 mm/yr (Pérouse & Wernicke, 2017). The slip rate of the Boulder Front fault (0.26mm/yr) is directly in line with the regional values.

5.3. *Regional Erosion and Uplift Relationships*

Erosion rates in catchments north of Galena Summit (Samples 1-4) yielded no major differences when compared to those over 80km SE in the upper Wood River Valley (Samples 5-7). (Figure 13). Additionally, larger drainage basins did not have distinctly different erosion rates than smaller drainage basins (Table 4). With the exception of the erosion rate from Crooked Creek catchment, the values are within about a two-fold range with an average erosion rate of 54.8±3.7 m/Myr. Diorite outcrops Crooked Creek catchment in its upper reaches with Quaternary terrace deposits and glacial deposits in its lower and middle reaches (Killsgaard et

al., 2006). These coverages are comparable to those near Boulder Creek, a catchment of similar size. Boulder Creek catchment consists of igneous and sedimentary rocks in its upper/middle reaches and alluvial and glacial deposits in its lower catchment (Lewis et al., 2012). Rock-type underlying the catchment does not reveal a significant enough difference to warrant the higher Crooked Creek erosion rate. A recent landslide within the Crooked Creek catchment may be the distinguishing factor between the higher erosion rate (183±15 m/Myr) and those of the other catchments (40.8±3.5 m/Myr-82.2±6.8 m/Myr). Overall, these values are mostly in line with regional erosion rates for the Northern Basin and Range which are about 20-100 m/Myr (Mitchell et al., 2023).

A defining feature of these mountain ranges in the Northern Basin and Range is glaciation shaping the landscapes (Easterbrook et al., 2011). Studies of erosion rates in the Northern Basin and Range in the Rocky Mountains of Colorado and Wyoming show glaciated environments having erosion rates of 40 m/Myr with unglaciated environments having erosion rates of 23-75 m/Myr (Dethier et al., 2014). Although these values are slightly lower than some of the erosion rates calculated for central Idaho, they reveal that no major differences exist amongst the erosion rates in catchments that experienced late Pleistocene glaciations.

Modeled results presented in the uplift rate graphs of Figure 15 only account for the recent ~75% of the modeled data as most iterations of the older timesteps did not yield any data and were therefore excluded. The maximum response time of the graphs presented indicate base-level fall in the stream channel reaching the headwaters where there is an absence of fluvial processes (Figure 15; Fisher et al., 2022). In the last half a million years there has been a clear decline in modeled uplift rates towards present-day implying a possible decrease in tectonic activity as compared to historic rates. In the Boulder Creek catchment, uplift rates appear to be

relatively steady around 6 Myr and later. Minor increases in uplift rate to 0.11 mm/yr exist at 3.25 Myr and 4.25 Myr, but no order of magnitude changes that would indicate high rates of past tectonic activity.

Catchment-scale modeling reveals differences amongst catchments with visible fault scarps and those where they are absent. Crooked Creek and Boulder Creek catchment are the only two catchments in the study where a visible fault scarp is present (Table 4; Figure 15b and 15g; Lifton et al, 2023; Boyle et al., 2023). Huckleberry Creek catchment, despite being situated along the Sawtooth fault, has only an inferred scarp in its upper reaches (Thackray, 2013). Comparisons of modeled present-day rates in Figure 15 show uplift to be much higher than those of the other catchments with Boulder Creek being 0.07 mm/yr and Crooked Creek being 0.08 mm/yr. With the exception of Lola Creek, the catchments with visible fault scarps have uplift rates of 3.5-4 times those of catchments with no evidence of faulting. This leads to the implication that these ground-rupturing faults may have an influence on the local uplift of these catchments (Crone & Haller, 1991). However, with all the uplift rates being in the same order of magnitude, it is likely this area of central Idaho is being driven by the larger-scale regional uplift of the Northern Basin and Range. Additionally, with the erosion rates of all catchments being higher than their respective uplift rates, it is demonstrating the gentle slope of the stream towards the mouth of the stream.

Lola Creek catchment has a present-day uplift rate of 0.05mm/yr and is the only other drainage basin with a rate above 0.2mm/yr. Although no visible scarp was observed, it is found along strike of the northwestern extension of the main branch of the Sawtooth fault and is situated 9.5 km to the southeast of the epicenter of the 2020 Stanley earthquake (Lifton et al.,

2023). Additional studies could look into the eastern front of Cape Horn Mountain where the Sawtooth fault may be extended to the north (Figure 1).

6. Conclusion

The SW-dipping Boulder Front fault situated in the Centennial Tectonic Belt within the Northern Basin and Range Province is characterized as a range-bounding normal fault in the upper Wood River Valley. Surficial geologic mapping and DEM interpretation delineate 7 separate segments over the 20 km strike-length of the Boulder Front fault. Lack of continuous scarps and differences in strike orientations divide these segments into the northwestern, central, and southeastern sections. The differing physical properties leads to the conclusion that the entire Boulder Front fault likely did not rupture at the same time, but all of segment 6 at Boulder Creek did. Seismic hazard exists for Ketchum and Sun Valley, Idaho based on the length of the scarps with correlation predicting M5.7 earthquakes estimated for the Boulder Creek segment. Recurrence intervals of approximately 2.3kyr are calculated from diffusional modeling and radiocarbon sampling showing at least two ground-rupturing earthquakes in the last 3-7kyr, with slip measurements implying ~7 previous events throughout the late Pleistocene. Radiocarbon data also suggests a recent rupture of the most northwestern segment in the last ~1,100yrs. The difference in rupture age reinforces that the sections are not linked at depth. Erosion rate analysis reveals no distinct differences between catchments based on drainage area, geographic location, or glacial activity and rates are in line with regional values of the Northern Basin and Range. Present-day uplift rates in catchments with visible fault scarps are 3.5-4 times higher than those without a fault scarp, with the exception of Lola Creek catchment. Regional uplift in the Northern Basin and Range Province is the driving force of uplift of these individual catchments in central Idaho.

References Cited

Anastasio, D.J., Majerowicz, C. N., Pazzaglia, F.J., & Regalla, C. A. (2010). Late Pleistocene - Holocene Ruptures of the Lima Reservoir Fault, SW Montana. *Journal of Structural Geology*, *32*(12), 1996-2008. https://doi.org/10.1016/j.jsg.2010.08.012

Balco, G., Stone, J.O., Lifton, N.A., & Dunai, T.J. (2008). A complete and easily accessible means of calculating surface exposure ages or erosion rates from $_{10}$Be and $_{26}$Al measurements. *Quaternary Geology*, *3*(3), 174-195. https://doi.org/10.1016/j.quageo.2007.12.001

Belmont, P., Pazzaglia, F.J., & Gosse, J.C. (2007). Cosmogenic ^{10}Be as a tracer for hillslope and channel sediment dynamics in the Clearwater River, western Washington State. *Earth and Planetary Science Letters*, *264*(1-2), 123-135. https://doi.org/10.1016/j.epsl.2007.09.013

Boyle, S., Nowak, T., Berti, C., & Anastasio, D.J. (2023). Fault Segmentation and Analysis of the Rupture History of the Boulder Front Fault, Northern Basin and Range Province, Idaho. *Geologic Society of America Abstracts with Programs*, *55*(6). http://doi.org/10.1130/abs/2023AM-391640

Cowie, P.A. (1998). A healing-reloading feedback control on the growth rate of seismogenic faults. *Journal of Structural Geology*, *20*(8), 1075-1087. https://doi.org/10.1016/S0191-8141(98)00034-0

Crone, A.J., & Haller, K.M. (1991). Segmentation and the coseismic behavior of Basin and Range normal faults: examples from east-central Idaho and southwestern Montana, U.S.A. *Journal of Structural Geology*, *13*(2), 151-164.

Crone A.J., Haller, K.M., & Lewis., R.S. (2010). Fault number 640, Sawtooth fault, in Quaternary fault and fold database of the United States, *U.S. Geological Survey website*. https://earthquake.usgs.gov/static/lfs/nshm/qfaults/Reports/640.pdf

Crone, A.J., & Neier, R.S. (2010). Fault number 639, Boulder front fault, in Quaternary fault and fold database of the United States, *U.S. Geological Survey website*. https://earthquake.usgs.gov/cfusion/qfault/show_report_AB_archive.cfm?fault_id=639§oid=

Dethier, D.P., Ouimet, W., Bierman, P.R., Rood, D.H., & Balco, G. (2014). Basin and bedrock: Spatial variation in ^{10}Be erosion rates and increasing relief in the southern Rocky Mountains, USA. Geology, *42*(2), 167-170. https://doi.org/10.1130/G34922.1

Di Bucci, D., Massa, B., & Zuppetta, A. (2006). Relay ramps in active normal fault zones; a clue to the identification of seismogenic sources (1688 Sannio earthquake, Italy). *Geological Society of America Bulletin, 118*(3-4), 430-448. https://doi.org/10.1130/B25783.1

Easterbrook, D.J., Gosse, J., Sherard, C., Evenson, E., & Finkel, R. (2011). Evidence for synchronous global climatic Events: Cosmogenic Exposure Ages of Glaciations. *Evidence-Based Climate Science*, Chapter 2, 53-88. https://doi.org/10.1016/B978-0-12-385956-3.10002-6

Idaho Lidar Consortium. (2021). www.idaholidar.org/.

Idaho Office of Emergency Management. (2019). 1983 Borah Peak Earthquake, *Earthquakes*. https://ioem.idaho.gov/news/a-history-of-idaho-disasters/earthquakes/

Fisher, J.A., Pazzaglia, F.J., Anastasio, D.J., & Gallen, S.F. (2022). Linear inversion of fluvial topography in the northern Apennines: comparison of base-level fall to crustal shortening. *Tectonics*, *41*(11). https://doi.org/10.1029/2022TC007379

Gans, P.B., & Bohrson, W.A. (1998). Suppresion of Volcanism During Rapid Extension in the Basin and Range Province, United States. *Science*, *279*(5347), 66-68. https://doi.org/10.1126/science.279.5347.66

Goren, L., Fox, M., & Willett, S.D. (2014). Tectonics from fluvial topography using formal linear inversion: Theory and applications to the Inyo Mountains, California. *JGR Earth Surface*, *119*(8), 1651-1681. https://doi.org/10.1002/2016GL070451

Granger, D.E., Kirchner, J.W., & Finkel, R. (1996). Spatially averaged long-term erosion rates measured from in situ-produced cosmogenic nuclides in alluvial sediment. *The Journal of Geology*, *104*(3), 249-257. https://doi.org/10.1086/629823

Harkins, N. W., Anastasio, D.J. & Pazzaglia, F.J. (2005). Tectonic geomorphology of the Red Rock fault, insights into segmentation and landscape evolution of a developing range front normal Fault. *Journal of Structural Geology*, *27*(11), 1925–1939. https://doi.org/10.1016/j.jsg.2005.07.005

Hanks, T.C. (2000). The Age of Scarplike Landforms From Diffusion-Equation Analysis. *Quaternary Geochronology: Methods and Applications*, *4*, 313-338. https://doi.org/10.1029/RF004p0313

Hilley, G.E., Arrowsmith, R., & Amoroso, L. (2001). Interaction between normal faults and fractures and fault scarp morphology. *Geophysical Research Letters*, *28*(19), 3777-3780. https://doi.org/10.1029/2001GL012876

Jackson, J.A., & White N.J. (1989). Normal faulting in the upper continental crust: observations from regions of active extension. *Journal of Structural Geology*, *11*(1-2), 15-36. https://doi.org/10.1016/0191-8141(89)90033-3

Killsgaard, T.H., Loudon, R.S., & Lewis, R.S. (2006). Geologic Map of the Daedwood River 30 x 60 Minute Quadrangle. *Idaho Geological Survey*. GM-45. https://www.idahogeology.org/product/gm-45

Kirby, E., Whipple, K.X., Tang, W., & Chen, Z. (2003). Distribution of active rock uplift along the eastern margin of the Tibetan Plateau: Inferences from bedrock channel longitudinal profiles. *JGR Solid Earth*, *108*(B4). https://doi.org/10.1029/2001JB000861

Lewis, R.S., Link, P.K., Stanford., L.R., & Long, S. (2012). Geologic Map of Idaho. *Idaho Geological Survey*. https://www.idahogeology.org/product/m-9

Liberty, L.M., Lifton, Z.M., & Mikesell, T.D. (2021). The 31 March 2020 Mw 6.5 Stanley, Idaho, earthquake: Seismotectonics and preliminary aftershock analysis. *Seismological Research Letters*, *92*(2A), 663–678. https://doi.org/10.1785/0220200319

Lifton, Z.M., Zellman, M.S., & Thackray, G.D. (2023). Surface Fault Scarp Mapping of the Sawtooth Fault, Central Idaho. *Idaho Geological Survey Staff Reports*, S-23-03. https://www.idahogeology.org/pub/Staff_Reports/S-23-03_Sawtooth_Fault_Report.pdf

Link, P.K., Mahoney, J.B., Bruner, D.J., Batatian, L.D., Wilson, E., & Williams, J.C. (1995). Geologic Map of Outcrop Areas of Sedimentary Units in the Eastern Part of the Hailey 1° x 2° Quadrangle and Part of the Southern Part of the Challis 1° x 2° Quadrangle, South-Central Idaho. *U.S. Geological Survey*, Bulletin 2064-C, Plate 1. https://pubs.usgs.gov/bul/b2064-c/

Liu, M., & Shen., Y. (1998). Crustal collapse, mantle upwelling, and Cenozoic extension in the North American Cordillera. *Tectonics*, *17*(2), 311-321. https://doi.org/10.1029/98TC00313

Mattson, A., & Bruhn, R.L. (2001). Fault slip rates and initiation age based on diffusion equation modeling: Wasatch Fault Zone and eastern Great Basin. *Journal of Geophysical Research*, *106*(B7), 13739-13750. https://doi.org/10.1029/2001JB900003

Mitchell, N., Yanites, B., Duvall, A., Humphreys, E., Perry-Houts, J., Schoettle-Greene, P., & Williams, S. (2023). Late Miocene or older canyon incision in the northern U.S. Cordillera shown by erosion rates, incision models and basalt flow ages. *GSA Bulletin*, *135*(11-12), 3143-3162. https://doi.org/10.1130/B36524.1

Morell, K.D., Styron, R., Stirling, M., Griffin, J., Archuleta, R., & Onur, T. (2020). Seismic Hazard Analyses From Geologic and Geomorphic Data: Current and Future Challenges. *Tectonics*, *39*(10). https://doi.org/10.1029/2018TC005365

Nash, D.B. (2005). A general method for morphologic dating of hillslopes. *Geology*, *33*(8) 693-695. https://doi.org/10.1130/G21479AR.1

Nash, D. B. (1986). Morphologic dating and modeling degradation of fault scarps. *Active tectonics: Impact on Society*, Chapter 12, 181-194. https://nap.nationalacademies.org/read/624/chapter/14

Newmann, J.R. (2019). Structural Evolution of an Extensional Terrane Margin: Case Studies from the Colorado Extensional Corridor, Southeastern California, USA. [M.Sc. thesis]: *UC Santa Barbara*. https://doi.org/10.13140/RG.2.2.34602.24005

Osborn G. (2024). Recognition of crustal extension in the Basin and Range Province: A history. *Geosphere*, *20*(5), 1247-1275 https://doi.org/10.1130/GES02758.1

Payne, S.J., McCaffrey, R., & Kattenhorn, S.A. (2013). Extension-driven right-lateral shear in the Centennial shear zone adjacent to the eastern Snake River Plain, Idaho. *Lithosphere*, *5*(4) 407-419. https://doi.org/10.1130/L200.1

Pérouse, E., & Wernicke, B.P. (2017). Spatiotemporal evolution of fault slip rates in deforming continents: The case of the Great Basin region, northern Basin and Range province. *Geosphere*, *13*(1), 112-135. https://doi.org/10.1130/GES01295.1

Pierce, K.L. (2003). Pleistocene glaciations of the Rocky Mountains. *Developments in Quaternary Sciences*, *1*, 63-76. https://doi.org/10.1016/S1571-0866(03)01004-2

Pierce, K.L., & Colman, S.M. (1986). Effect of height and orientation (microclimate) on geomorphic degradation rates and processes, late-glacial terrace scarps in central Idaho.

Geological Society of America Bulletin, *97*(7), 869-885. https://doi.org/10.1130/0016-7606(1986)97<869:EOHAOM>2.0.CO;2

Regalla, C. A., Anastasio, D. J., & Pazzaglia, F. J. (2007). Characterization of the Monument Hill fault system and implications for the active tectonics of the Red Rock Valley, Southwestern Montana. *Journal of Structural Geology*, *29*(8), 1339-1352. https://doi.org/10.1016/j.jsg.2007.04.006

Schwanghart, W. & Scherler, D. (2014). Short Communication: TopoToolbox 2 – MATLAB-based software for topographic analysis and modeling in Earth surface sciences. *Earth Surface Dynamics*, *2*(1)1–7. https://doi.org/10.5194/esurf-2-1-2014

Schwartz, D.P., & Coppersmith, K.J. (1984). Fault behavior and characteristic earthquakes: Examples from the Wasatch and San Andreas Fault Zones. *JGR Solid Earth*. *89*(B7), 5681-5698. https://doi.org/10.1029/JB089iB07p05681

Stewart, I.S., & Hanock, P.L. (1990). What is a fault scarp? *Episodes*, *13*(4), 256-263. https://doi.org/10.18814/epiiugs/1990/v13i4/005

Stickney, M.C., (1993). Seismicity and focal mechanisms of the central Centennial Tectonic Belt, southwestern Montana and east-central Idaho. *Geological Society of America, Abstract with Programs*, *25*(5). https://www.osti.gov/biblio/5022779

Stickney, M.C., & Bartholomew, M.J. (1987). Seismicity and late Quaternary faulting of the northern basin and range province, Montana and Idaho. *Bulletin of the Seismological Society of America*, *77*(5), 1602-1625. https://doi.org/10.1785/BSSA0770051602

Stirling, M., Rhoades, D., & Berryman, K. (2002). Comparison of Earthquake Scaling Relations Derived from Data of the Instrumental and Preindustrial Era. *Bulletin of the Seismological Society of America*, *92*(2), 812-830. https://doi.org/10.1785/0120000221

Thackray, G.D., Rodgers, D.W., & Streutker, D. (2013). Holocene scarp on the Sawtooth fault, central Idaho, USA, documented through lidar topographic analysis. *Geology*, *41*(6), 639-642. https://doi.org/10.1130/G34095.1

Wells, D.L., & Coppersmith, K. J. (1994). New Empirical Relationships among Magnitude, Rupture Length, Rupture Width, Rupture Area, and Surface Displacement. *Bulletin of the Seismological Society of America*, *84*(4), 974-1002. https://doi.org/10.1785/BSSA0840040974

Wesnousky, S.G. (2008). Displacement and Geometrical Characteristics of Earthquake Surface Ruptures: Issues and Implications for Seismic-Hazard Analysis and the Process of Earthquake Rupture. *Bulletin of the Seismological Society of America*, *98*(4), 1609-1632. https://doi.org/10.1785/0120070111

Williams, P.L. (1961). Glacial geology of the Stanley Basin: Moscow, Idaho Bureau of Mines and Geology. *Idaho Geological Survey*, P-123. https://www.idahogeology.org/product/p-123

Appendix A

Surficial Geologic Map and Unit Descriptions

[Qal] *Alluvium*: Organic rich, dark brown soil. Silt-medium sand grain size. Matrix-supported. Some well-sorted, rounded-sub rounded pebbles, 0.5cm-2cm. Found in active stream channels.

[Qls] *Landslide*: Silt-coarse sand grain size. Poorly-sorted, angular clasts. Found along bedrock slopes.

[Qaf] *Alluvial Fan*: Tan to light brown color. Silt-coarse sand grain size. Clast-supported. Granitic, moderately well-sorted, sub rounded-sub angular pebbles, 0.5cm-1cm with a few cobbles up to 20 cm. Some boulders, less than 1m with the average being 0.25-0.5m. Grain size fines and is more matrix-supported towards the lower drainage area.

[Qdf] *Debris Flow*: Silt-coarse sand grain size. Poorly-sorted, sub rounded to angular clasts. Found in stream channels.

[Qt4] *Terrace 4*: Darker brown color. Silt-coarse sand grain size. Matrix-supported. Moderately well-sorted, rounded pebbles and cobbles, 0.5cm-10cm. Some boulders, 0.25m-0.3m.

[Qt3] *Terrace 3*: Moderate brown color. Silt-coarse sand grain size. Matrix-supported. Moderately-poorly sorted, sub rounded-rounded pebbles, 0.5cm-5cm. Well-sorted boulders, 0.25m-0.5m.

[Qt2] *Terrace 2*: Moderate-dark brown color. Silt-coarse sand grain size. Matrix-supported. Well-sorted, sub rounded pebbles, 0.5cm-2cm. Few boulders, 0.25m-0.3m

[Qt1] *Terrace 1*: Moderate brown color. Silt-medium sand grain size. Matrix-supported. Many moderately well-sorted, sub rounded pebbles, 0.5cm-5cm. Scattered boulders less than 1.5m.

[Qcl] *Colluvium*: Light brown color. Silt-coarse sand grain size. Matrix-supported. Moderately well-sorted, angular, 0.5cm-5cm pebbles.

[Qc] *Colluvium Overlying Bedrock*: Colluvium (Qcl) overlying bedrock (Bdr) hillslopes.

[Qpo] *Pinedale Outwash*: Moderate-dark brown color. Silt-medium sand grain size. Clast-supported. Well-sorted, sub angular-sub rounded pebbles, 0.5cm-3cm. Few boulders, 0.5m-1.5m.

[Qpt] *Pinedale Moraine*: Tan-light brown color. Silt-coarse sand grain size. Matrix-supported. Poorly-sorted, sub angular-sub rounded pebbles, 1cm-6cm. Scattered boulders with pink-coloring, 0.5m-1.5m.

[Qbo] *Bull Lake Outwash*: Moderate brown color. Fine-medium sand grain size. Matrix-supported. Moderately-poorly sorted, sub rounded pebbles, 1cm-5cm. Isolated boulders, 0.5m-1m.

[Qpt] *Bull Lake Moraine*: Moderate brown and dark gray color. Silt-coarse sand grain size. Matrix-supported. Poorly sorted, sub angular pebbles, 1cm-5cm. Sub angular boulders 0.25m-0.3m with a few 1m boulders.

[QTg] *Tertiary Gravel*: Tan to light brown color. Silt-coarse sand grain size. Clast-supported. Poorly sorted, sub rounded-rounded pebbles and cobbles, 1-15cm. Few boulders, 0.3m-0.5m.

[Bedrock] *Bedrock*: Bedrock is not differentiated on the map for this project. Tertiary igneous rocks (Eocene): Challis Volcanic Group and Intrusive rocks (granite, rhyolite porphyry, dacite porphyry and granodiorite). Paleozoic sedimentary rock (Lower Permian to Middle Pennsylvanian): Wood River Formation, Eagle Creek Member (Link et al., 1995).

Surficial Geologic Map of Parts of the Easley Hot Springs and Amber Lakes 7.5' Quadrangles, Idaho

Principal Field Mapper: Sedona Boyle
Field Assistant: Tabitha Nowak
Lehigh University, Bethlehem, PA

2024

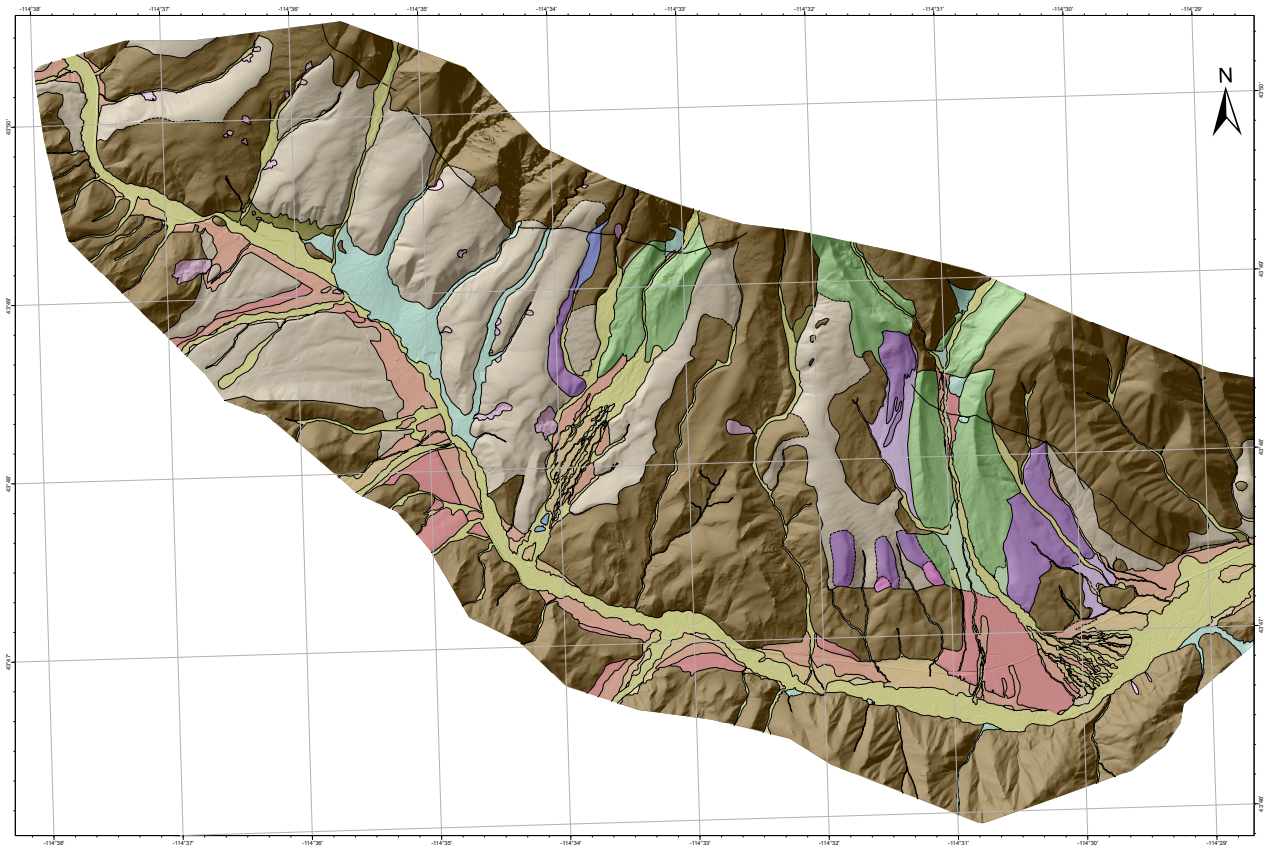

Scale: 1:24,000

0 0.5 1 2 3 4 Kilometers

0 0.5 1 2 3 4 Miles

Surficial Units

Lake — Water feature.

Qal — Alluvium: Organic rich, dark brown soil. Silt-medium sand grain size. Matrix-supported. Some well-sorted, rounded-sub rounded pebbles, 0.5cm-2cm. Found in active stream channels.

Qls — Landslide: Silt-coarse sand grain size. Poorly-sorted, angular clasts. Found along bedrock slopes.

Qaf — Alluvial Fan: Tan to light brown color. Silt-coarse sand grain size. Clast-supported. Granitic, moderately well-sorted, sub rounded-sub angular pebbles, 0.5cm-1cm with a few cobbles up to 20cm. Some boulders, less than 1m with the average being 0.25cm-0.5m. Grain size fines and is more matrix-supported towards the lower drainage area.

Qdf — Debris Flow: Silt-coarse sand grain size. Poorly-sorted, sub rounded to angular clasts. Found in stream channels.

Qt4 — Terrace 4: Darker brown color. Silt-coarse sand grain size. Matrix-supported. Moderately well-sorted, rounded pebbles and cobbles, 0.5cm-10cm. Some boulders, 0.25m-0.3m.

Qt3 — Terrace 3: Moderate brown color. Silt-coarse sand grain size. Matrix-supported. Moderately-poorly sorted, sub rounded-rounded pebbles, 0.5cm-5cm. Well-sorted boulders, 0.25m-0.5m.

Qt2 — Terrace 2: Moderate-dark brown color. Silt-coarse sand grain size. Matrix-supported. Well-sorted, sub rounded pebbles, 0.5cm-2cm. Few bouders, 0.25m-0.3m.

Qt1 — Terrace 1: Moderate brown color. Silt-medium sand grain size. Matrix-supported. Many moderately well-sorted, sub rounded pebbles, 0.5cm-5cm. Scattered boulders less than 1.5m.

Qcl — Colluvium: Light brown color. Silt-coarse sand grain size. Matrix-supported. Moderately well-sorted, angular, 0.5cm-5cm pebbles.

Qc — Colluvium (Qcl) overlying bedrock hillslopes.

Qpo — Pinedale Outwash: Moderate-dark brown color. Silt-medium sand grain size. Clast-supported. Well-sorted, sub angular-sub rounded pebbles, 0.5cm-3cm. Few boulders, 0.5m-1.5m.

Qpt — Pinedale Moraine: Tan-light bown color. Silt-coarse sand grain size. Matrix-supported. Poorly-sorted, sub angular-sub rounded pebbles, 1cm-6cm. Scattered boulders with pink coloring, 0.5m-1.5m.

Qbo — Bull Lake Outwash: Moderate brown color. Fine-medium sand grain size. Matrix-supported. Moderately-poorly sorted, sub rounded pebbles, 1cm-5cm. Isolated boulders, 0.5m-1m.

Qbt — Bull Lake Moraine: Moderate brown and dark gray color. Silt-coarse sand grain size. Matrix-supported. Poorly sorted, sub angular pebbles, 1cm-5cm. Sub angular boulders, 0.25m-0.3m, with a few 1m boulders.

QTg — Tertiary Gravel: Tan to light brown color. Silt-coarse sand grain size. Clast-supported. Poorly-sorted, sub rounded-rounded pebbles and cobbles, 1-15cm. Few boulders, 0.3m-0.5m.

Bedrock — Bedrock is not differentiated on the map for this project. Tertiary igneous rocks (Eocene): Challis Volcanic Group and Intrusive rocks (granite, rhyolite porphyry, dacite porphyry and granodiorite) Paleozoic sedimentary rocks (Lower Permian-Middle Pennsylvanian): Wood River Formation, Eagle Creek Member.

Faculty Advisors: Dr. David Anastasio (Lehigh University) and Dr. Claudio Berti (Idaho Geological Survey and the University of Idaho)

Fieldwork conducted 2023-2024.

This surficial map was funded by the EDMAP Program of the National Cooperative Geologic Mapping Program of the U.S. Geological Survey under Grant Number: G22AC00177-00.

Map Symbols

- Fault
- Inferred Fault
- Buried Fault
- Contact
- Inferred Contact

Appendix B

Radiocarbon Data

The results of the radiocarbon dating from Beta Analytic Testing Laboratory are attached below and include the conventional radiocarbon age and the calibration of the radiocarbon age to calendar years.

Beta Analytic, Inc.
4985 SW 74th Court
Miami, FL 33155 USA
Tel: 305-667-5167
Fax: 305-663-0964
info@betalabservices.com

ISO/IEC 17025:2017-Accredited Testing Laboratory

REPORT OF RADIOCARBON DATING ANALYSES

Claudio Berti — Report Date: July 01, 2024

Idaho Geological Survey — Material Received: June 20, 2024

Laboratory Number	Sample Code Number	Conventional Radiocarbon Age (BP) or Percent Modern Carbon (pMC) & Stable Isotopes	
Beta - 700029	**23CB002**	**1190 +/- 30 BP**	IRMS δ13C: -23.4 o/oo
(87.9%)	**770 - 896 cal AD**	**(1180 - 1054 cal BP)**	
(5.8%)	**922 - 952 cal AD**	**(1028 - 998 cal BP)**	
(1.6%)	**708 - 722 cal AD**	**(1242 - 1228 cal BP)**	

Submitter Material: Charcoal
Pretreatment: (charred material) acid/alkali/acid
Analyzed Material: Charred material
Analysis Service: AMS-Standard delivery
Percent Modern Carbon: 86.23 +/- 0.32 pMC
Fraction Modern Carbon: 0.8623 +/- 0.0032
D14C: -137.69 +/- 3.22 o/oo
Δ14C: -145.37 +/- 3.22 o/oo (1950:2024)
Measured Radiocarbon Age: (without d13C correction): 1160 +/- 30 BP
Calibration: BetaCal5.0: HPD method: INTCAL20

Results are ISO/IEC-17025:2017 accredited. No sub-contracting or student labor was used in the analyses. All work was done at Beta in 4 in-house NEC accelerator mass spectrometers and 4 Thermo IRMSs. The "Conventional Radiocarbon Age" was calculated using the Libby half-life (5568 years), is corrected for total isotopic fraction and was used for calendar calibration where applicable. The Age is rounded to the nearest 10 years and is reported as radiocarbon years before present (BP), "present" = AD 1950. Results greater than the modern reference are reported as percent modern carbon (pMC). The modern reference standard was 95% the 14C signature of NIST SRM-4990C (oxalic acid). Quoted errors are 1 sigma counting statistics. Calculated sigmas less than 30 BP on the Conventional Radiocarbon Age are conservatively rounded up to 30. d13C values are on the material itself (not the AMS d13C). d13C and d15N values are relative to VPDB. References for calendar calibrations are cited at the bottom of calibration graph pages.

BetaCal 5.0

Calibration of Radiocarbon Age to Calendar Years

(High Probability Density Range Method (HPD): INTCAL20)

(Variables: d13C = -23.4 o/oo)

Laboratory number **Beta-700029**

Conventional radiocarbon age **1190 ± 30 BP**

95.4% probability

(87.9%)	770 - 896 cal AD	(1180 - 1054 cal BP)
(5.8%)	922 - 952 cal AD	(1028 - 998 cal BP)
(1.6%)	708 - 722 cal AD	(1242 - 1228 cal BP)

68.2% probability

(54.4%)	821 - 886 cal AD	(1129 - 1064 cal BP)
(13.8%)	774 - 790 cal AD	(1176 - 1160 cal BP)

23CB002

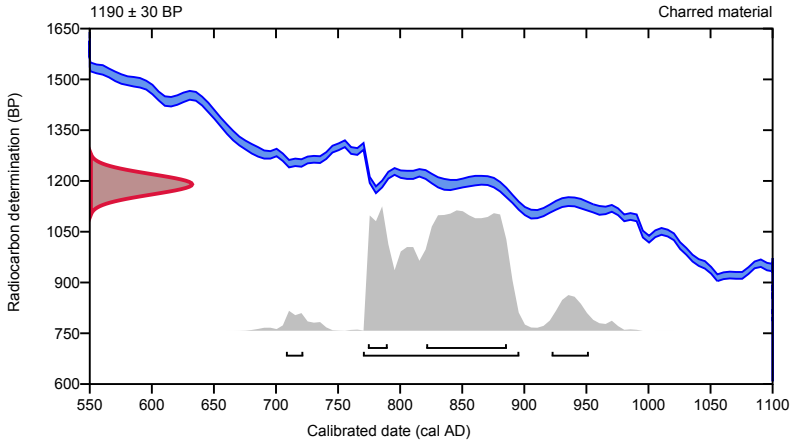

Database used

INTCAL20

References

References to Probability Method

Bronk Ramsey, C. (2009). Bayesian analysis of radiocarbon dates. Radiocarbon, 51(1), 337-360.

References to Database INTCAL20

Reimer, et al., 2020, Radiocarbon 62(4):725-757.

Beta Analytic, Inc.
4985 SW 74th Court
Miami, FL 33155 USA
Tel: 305-667-5167
Fax: 305-663-0964
info@betalabservices.com

ISO/IEC 17025:2017-Accredited Testing Laboratory

REPORT OF RADIOCARBON DATING ANALYSES

Claudio Berti — Report Date: July 01, 2024

Idaho Geological Survey — Material Received: June 20, 2024

Laboratory Number	Sample Code Number	Conventional Radiocarbon Age (BP) or Percent Modern Carbon (pMC) & Stable Isotopes	
Beta - 700030	**23CB003**	**4020 +/- 30 BP**	IRMS δ13C: -20.7 o/oo

(90.4%) 2584 - 2467 cal BC (4533 - 4416 cal BP)
(5.0%) 2622 - 2599 cal BC (4571 - 4548 cal BP)

Submitter Material: Charcoal
Pretreatment: (charred material) acid/alkali/acid
Analyzed Material: Charred material
Analysis Service: AMS-Standard delivery
Percent Modern Carbon: 60.63 +/- 0.23 pMC
Fraction Modern Carbon: 0.6063 +/- 0.0023
D14C: -393.74 +/- 2.26 o/oo
Δ14C: -399.14 +/- 2.26 o/oo (1950:2024)
Measured Radiocarbon Age: (without d13C correction): 3950 +/- 30 BP
Calibration: BetaCal5.0: HPD method: INTCAL20

Results are ISO/IEC-17025:2017 accredited. No sub-contracting or student labor was used in the analyses. All work was done at Beta in 4 in-house NEC accelerator mass spectrometers and 4 Thermo IRMSs. The "Conventional Radiocarbon Age" was calculated using the Libby half-life (5568 years), is corrected for total isotopic fraction and was used for calendar calibration where applicable. The Age is rounded to the nearest 10 years and is reported as radiocarbon years before present (BP), "present" = AD 1950. Results greater than the modern reference are reported as percent modern carbon (pMC). The modern reference standard was 95% the 14C signature of NIST SRM-4990C (oxalic acid). Quoted errors are 1 sigma counting statistics. Calculated sigmas less than 30 BP on the Conventional Radiocarbon Age are conservatively rounded up to 30. d13C values are on the material itself (not the AMS d13C). d13C and d15N values are relative to VPDB. References for calendar calibrations are cited at the bottom of calibration graph pages.

BetaCal 5.0

Calibration of Radiocarbon Age to Calendar Years

(High Probability Density Range Method (HPD): INTCAL20)

(Variables: d13C = -20.7 o/oo)

Laboratory number **Beta-700030**

Conventional radiocarbon age **4020 ± 30 BP**

95.4% probability

(90.4%)	2584 - 2467 cal BC	(4533 - 4416 cal BP)
(5%)	2622 - 2599 cal BC	(4571 - 4548 cal BP)

68.2% probability

(32.1%)	2544 - 2511 cal BC	(4493 - 4460 cal BP)
(15.8%)	2573 - 2556 cal BC	(4522 - 4505 cal BP)
(15.4%)	2505 - 2489 cal BC	(4454 - 4438 cal BP)
(5%)	2482 - 2476 cal BC	(4431 - 4425 cal BP)

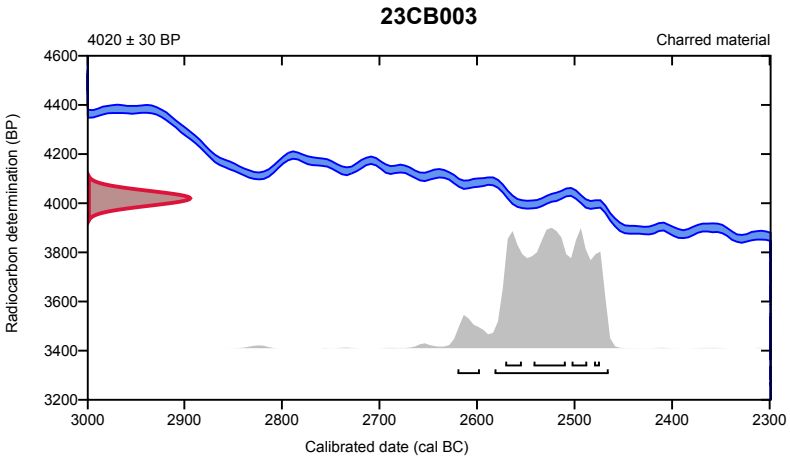

Database used

INTCAL20

References

References to Probability Method

Bronk Ramsey, C. (2009). Bayesian analysis of radiocarbon dates. Radiocarbon, 51(1), 337-360.

References to Database INTCAL20

Reimer, et al., 2020, Radiocarbon 62(4):725-757.

Beta Analytic, Inc.
4985 SW 74th Court
Miami, FL 33155 USA
Tel: 305-667-5167
Fax: 305-663-0964
info@betalabservices.com

ISO/IEC 17025:2017-Accredited Testing Laboratory

REPORT OF RADIOCARBON DATING ANALYSES

Claudio Berti — Report Date: July 01, 2024

Idaho Geological Survey — Material Received: June 20, 2024

Laboratory Number	Sample Code Number	Conventional Radiocarbon Age (BP) or Percent Modern Carbon (pMC) & Stable Isotopes	
Beta - 700031	**23CB004**	**1190 +/- 30 BP**	IRMS δ13C: -26.2 o/oo

(87.9%)	**770 - 896 cal AD**	**(1180 - 1054 cal BP)**
(5.8%)	**922 - 952 cal AD**	**(1028 - 998 cal BP)**
(1.6%)	**708 - 722 cal AD**	**(1242 - 1228 cal BP)**

Submitter Material: Charcoal
Pretreatment: (charred material) acid/alkali/acid
Analyzed Material: Charred material
Analysis Service: AMS-Standard delivery
Percent Modern Carbon: 86.23 +/- 0.32 pMC
Fraction Modern Carbon: 0.8623 +/- 0.0032
D14C: -137.69 +/- 3.22 o/oo
Δ14C: -145.37 +/- 3.22 o/oo (1950:2024)
Measured Radiocarbon Age: (without d13C correction): 1210 +/- 30 BP
Calibration: BetaCal5.0: HPD method: INTCAL20

Results are ISO/IEC-17025:2017 accredited. No sub-contracting or student labor was used in the analyses. All work was done at Beta in 4 in-house NEC accelerator mass spectrometers and 4 Thermo IRMSs. The "Conventional Radiocarbon Age" was calculated using the Libby half-life (5568 years), is corrected for total isotopic fraction and was used for calendar calibration where applicable. The Age is rounded to the nearest 10 years and is reported as radiocarbon years before present (BP), "present" = AD 1950. Results greater than the modern reference are reported as percent modern carbon (pMC). The modern reference standard was 95% the 14C signature of NIST SRM-4990C (oxalic acid). Quoted errors are 1 sigma counting statistics. Calculated sigmas less than 30 BP on the Conventional Radiocarbon Age are conservatively rounded up to 30. d13C values are on the material itself (not the AMS d13C). d13C and d15N values are relative to VPDB. References for calendar calibrations are cited at the bottom of calibration graph pages.

BetaCal 5.0

Calibration of Radiocarbon Age to Calendar Years

(High Probability Density Range Method (HPD): INTCAL20)

(Variables: d13C = -26.2 o/oo)

Laboratory number **Beta-700031**

Conventional radiocarbon age **1190 ± 30 BP**

95.4% probability

(87.9%)	770 - 896 cal AD	(1180 - 1054 cal BP)
(5.8%)	922 - 952 cal AD	(1028 - 998 cal BP)
(1.6%)	708 - 722 cal AD	(1242 - 1228 cal BP)

68.2% probability

(54.4%)	821 - 886 cal AD	(1129 - 1064 cal BP)
(13.8%)	774 - 790 cal AD	(1176 - 1160 cal BP)

23CB004

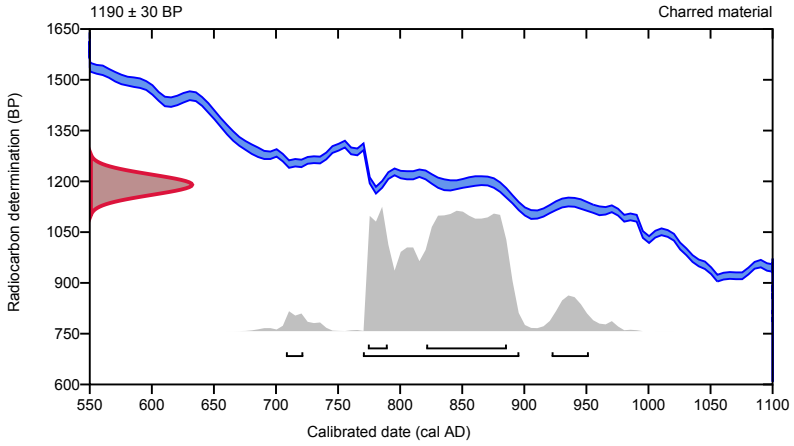

Database used

INTCAL20

References

References to Probability Method

Bronk Ramsey, C. (2009). Bayesian analysis of radiocarbon dates. Radiocarbon, 51(1), 337-360.

References to Database INTCAL20

Reimer, et al., 2020, Radiocarbon 62(4):725-757.

Beta Analytic, Inc.
4985 SW 74th Court
Miami, FL 33155 USA
Tel: 305-667-5167
Fax: 305-663-0964
info@betalabservices.com

ISO/IEC 17025:2017-Accredited Testing Laboratory

REPORT OF RADIOCARBON DATING ANALYSES

Claudio Berti — Report Date: July 01, 2024

Idaho Geological Survey — Material Received: June 20, 2024

Laboratory Number	Sample Code Number	Conventional Radiocarbon Age (BP) or Percent Modern Carbon (pMC) & Stable Isotopes	
Beta - 700028	**23CB001**	**2180 +/- 30 BP**	IRMS δ13C: -20.4 o/oo
(94.3%)	**364 - 150 cal BC**	**(2313 - 2099 cal BP)**	
(1.1%)	**131 - 121 cal BC**	**(2080 - 2070 cal BP)**	

Submitter Material: Charcoal
Pretreatment: (charred material) acid/alkali/acid
Analyzed Material: Charred material
Analysis Service: AMS-Standard delivery
Percent Modern Carbon: 76.23 +/- 0.28 pMC
Fraction Modern Carbon: 0.7623 +/- 0.0028
D14C: -237.68 +/- 2.85 o/oo
Δ14C: -244.47 +/- 2.85 o/oo (1950:2024)
Measured Radiocarbon Age: (without d13C correction): 2100 +/- 30 BP
Calibration: BetaCal5.0: HPD method: INTCAL20

Results are ISO/IEC-17025:2017 accredited. No sub-contracting or student labor was used in the analyses. All work was done at Beta in 4 in-house NEC accelerator mass spectrometers and 4 Thermo IRMSs. The "Conventional Radiocarbon Age" was calculated using the Libby half-life (5568 years), is corrected for total isotopic fraction and was used for calendar calibration where applicable. The Age is rounded to the nearest 10 years and is reported as radiocarbon years before present (BP), "present" = AD 1950. Results greater than the modern reference are reported as percent modern carbon (pMC). The modern reference standard was 95% the 14C signature of NIST SRM-4990C (oxalic acid). Quoted errors are 1 sigma counting statistics. Calculated sigmas less than 30 BP on the Conventional Radiocarbon Age are conservatively rounded up to 30. d13C values are on the material itself (not the AMS d13C). d13C and d15N values are relative to VPDB. References for calendar calibrations are cited at the bottom of calibration graph pages.

BetaCal 5.0

Calibration of Radiocarbon Age to Calendar Years

(High Probability Density Range Method (HPD): INTCAL20)

(Variables: d13C = -20.4 o/oo)

Laboratory number **Beta-700028**

Conventional radiocarbon age **2180 ± 30 BP**

95.4% probability

(94.3%)	364 - 150 cal BC	(2313 - 2099 cal BP)
(1.1%)	131 - 121 cal BC	(2080 - 2070 cal BP)

68.2% probability

(42%)	351 - 290 cal BC	(2300 - 2239 cal BP)
(23.3%)	209 - 174 cal BC	(2158 - 2123 cal BP)
(2.9%)	226 - 221 cal BC	(2175 - 2170 cal BP)

23CB001

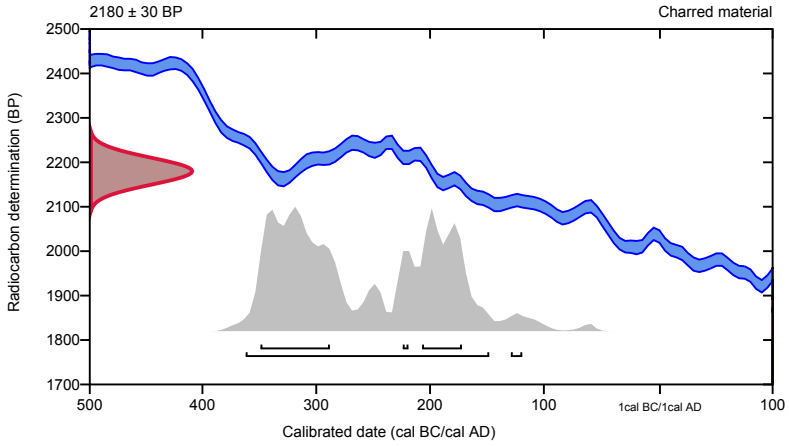

Database used

INTCAL20

References

References to Probability Method

Bronk Ramsey, C. (2009). Bayesian analysis of radiocarbon dates. Radiocarbon, 51(1), 337-360.

References to Database INTCAL20

Reimer, et al., 2020, Radiocarbon 62(4):725-757.

Beta Analytic, Inc.
4985 SW 74th Court
Miami, FL 33155 USA
Tel: 305-667-5167
Fax: 305-663-0964
info@betalabservices.com

ISO/IEC 17025:2017-Accredited Testing Laboratory

REPORT OF RADIOCARBON DATING ANALYSES

Claudio Berti — Report Date: October 07, 2021

Idaho Geological Survey — Material Received: September 22, 2021

Laboratory Number	Sample Code Number	Conventional Radiocarbon Age (BP) or Percent Modern Carbon (pMC) & Stable Isotopes	
Beta - 603712	**21CB003**	**2720 +/- 30 BP**	IRMS δ13C: -22.8 o/oo
(95.4%)	**919 - 809 cal BC**	**(2868 - 2758 cal BP)**	

Submitter Material: Organic Sediment/Gyttja
Pretreatment: (organic sediment) acid washes
Analyzed Material: Organic sediment
Analysis Service: AMS-Standard delivery
Percent Modern Carbon: 71.28 +/- 0.27 pMC
Fraction Modern Carbon: 0.7128 +/- 0.0027
D14C: -287.24 +/- 2.66 o/oo
Δ14C: -293.33 +/- 2.66 o/oo (1950:2021)
Measured Radiocarbon Age: (without d13C correction): 2680 +/- 30 BP
Calibration: BetaCal4.20: HPD method: INTCAL20

Results are ISO/IEC-17025:2017 accredited. No sub-contracting or student labor was used in the analyses. All work was done at Beta in 4 in-house NEC accelerator mass spectrometers and 4 Thermo IRMSs. The "Conventional Radiocarbon Age" was calculated using the Libby half-life (5568 years), is corrected for total isotopic fraction and was used for calendar calibration where applicable. The Age is rounded to the nearest 10 years and is reported as radiocarbon years before present (BP), "present" = AD 1950. Results greater than the modern reference are reported as percent modern carbon (pMC). The modern reference standard was 95% the 14C signature of NIST SRM-4990C (oxalic acid). Quoted errors are 1 sigma counting statistics. Calculated sigmas less than 30 BP on the Conventional Radiocarbon Age are conservatively rounded up to 30. d13C values are on the material itself (not the AMS d13C). d13C and d15N values are relative to VPDB. References for calendar calibrations are cited at the bottom of calibration graph pages.

BetaCal 4.20

Calibration of Radiocarbon Age to Calendar Years

(High Probability Density Range Method (HPD): INTCAL20)

(Variables: d13C = -22.8 o/oo)

Laboratory number **Beta-603712**

Conventional radiocarbon age **2720 ± 30 BP**

95.4% probability

(95.4%) 919 - 809 cal BC (2868 - 2758 cal BP)

68.2% probability

(68.2%) 898 - 827 cal BC (2847 - 2776 cal BP)

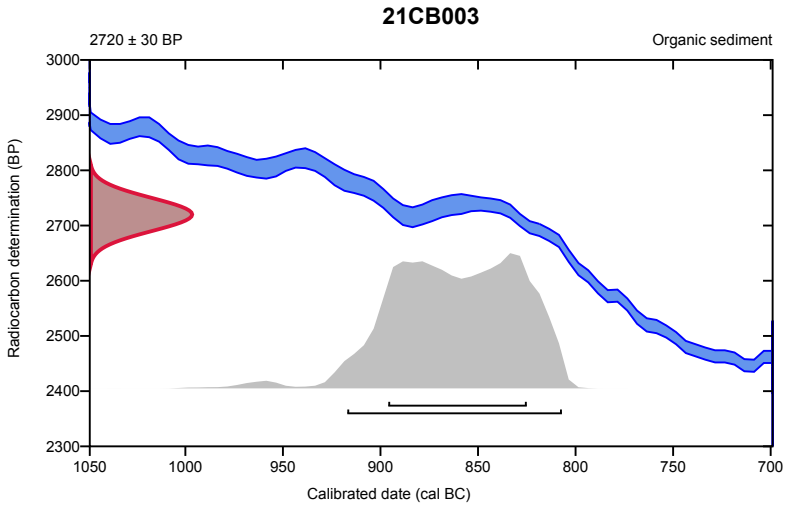

Database used

INTCAL20

References

References to Probability Method

Bronk Ramsey, C. (2009). Bayesian analysis of radiocarbon dates. Radiocarbon, 51(1), 337-360.

References to Database INTCAL20

Reimer, et al., 2020, Radiocarbon 62(4):725-757.

Beta Analytic Radiocarbon Dating Laboratory
4985 S.W. 74th Court, Miami, Florida 33155 • Tel: (305)667-5167 • Fax: (305)663-0964 • Email: beta@radiocarbon.com

Beta Analytic, Inc.
4985 SW 74th Court
Miami, FL 33155 USA
Tel: 305-667-5167
Fax: 305-663-0964
info@betalabservices.com

ISO/IEC 17025:2017-Accredited Testing Laboratory

REPORT OF RADIOCARBON DATING ANALYSES

Claudio Berti — Report Date: October 07, 2021

Idaho Geological Survey — Material Received: September 22, 2021

Laboratory Number	Sample Code Number	Conventional Radiocarbon Age (BP) or Percent Modern Carbon (pMC) & Stable Isotopes
Beta - 603711	**21CB002**	**3190 +/- 30 BP** IRMS δ13C: -22.2 o/oo
(95.4%)	**1507 - 1415 cal BC**	**(3456 - 3364 cal BP)**

Submitter Material: Charcoal
Pretreatment: (charred material) acid/alkali/acid
Analyzed Material: Charred material
Analysis Service: AMS-Standard delivery
Percent Modern Carbon: 67.23 +/- 0.25 pMC
Fraction Modern Carbon: 0.6723 +/- 0.0025
D14C: -327.74 +/- 2.51 o/oo
Δ14C: -333.49 +/- 2.51 o/oo (1950:2021)
Measured Radiocarbon Age: (without d13C correction): 3140 +/- 30 BP
Calibration: BetaCal4.20: HPD method: INTCAL20

Results are ISO/IEC-17025:2017 accredited. No sub-contracting or student labor was used in the analyses. All work was done at Beta in 4 in-house NEC accelerator mass spectrometers and 4 Thermo IRMSs. The "Conventional Radiocarbon Age" was calculated using the Libby half-life (5568 years), is corrected for total isotopic fraction and was used for calendar calibration where applicable. The Age is rounded to the nearest 10 years and is reported as radiocarbon years before present (BP), "present" = AD 1950. Results greater than the modern reference are reported as percent modern carbon (pMC). The modern reference standard was 95% the 14C signature of NIST SRM-4990C (oxalic acid). Quoted errors are 1 sigma counting statistics. Calculated sigmas less than 30 BP on the Conventional Radiocarbon Age are conservatively rounded up to 30. d13C values are on the material itself (not the AMS d13C). d13C and d15N values are relative to VPDB. References for calendar calibrations are cited at the bottom of calibration graph pages.

BetaCal 4.20

Calibration of Radiocarbon Age to Calendar Years

(High Probability Density Range Method (HPD): INTCAL20)

(Variables: d13C = -22.2 o/oo)

Laboratory number **Beta-603711**

Conventional radiocarbon age **3190 ± 30 BP**

95.4% probability

(95.4%) 1507 - 1415 cal BC (3456 - 3364 cal BP)

68.2% probability

(36%) 1464 - 1434 cal BC (3413 - 3383 cal BP)
(32.2%) 1498 - 1472 cal BC (3447 - 3421 cal BP)

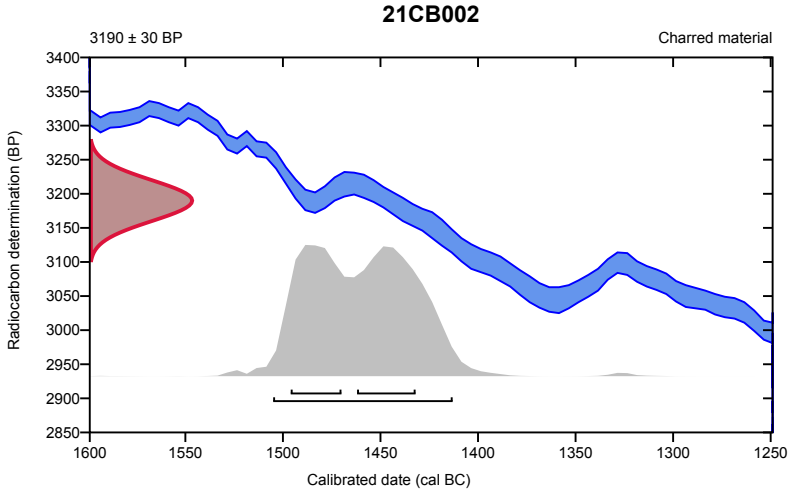

Database used

INTCAL20

References

References to Probability Method

Bronk Ramsey, C. (2009). Bayesian analysis of radiocarbon dates. Radiocarbon, 51(1), 337-360.

References to Database INTCAL20

Reimer, et al., 2020, Radiocarbon 62(4):725-757.

Beta Analytic Radiocarbon Dating Laboratory
4985 S.W. 74th Court, Miami, Florida 33155 • Tel: (305)667-5167 • Fax: (305)663-0964 • Email: beta@radiocarbon.com

Appendix C

Profile Data

Profile data for single slip and continuous slip diffusion modeling. Initial slope is set at 35**°.** Diffusion coefficient was modeled for $1.26x10^{-3}m^2/yr$ and $2.09\ x10^{-3}m^2/yr$. Half-slip rates were set at 0.10 mm/yr, 0.13 mm/yr and 0.16 mm/yr,

Profile	Half Offset (m)	Amount of Slip (m)	Scarp Slope (°)	Regional Slope (°)
1	2.20	4.40	35	7
2	2.80	5.60	34	7
3	2.30	4.60	N/A	5
4	0.37	0.74	16	3
5	2.50	5.00	27	9
6	2.08	4.16	15	12
7	2.95	5.90	N/A	5

Profile 1

```
0           2205.715
2.525240583 2205.922
5.09335273  2206.024
7.241878271 2206.167
9.3659689   2206.307
11.414791   2206.522
13.85318391 2206.68
15.98045917 2206.85
17.44967188 2206.998
19.78786434 2207.15
21.34707087 2207.148
22.71788122 2207.234
29.07287249 2207.758
31.38915226 2208.031
33.90734308 2208.276
36.31102796 2208.485
38.30063144 2208.655
40.13897009 2208.811
45.50664314 2209.168
47.68942417 2209.355
49.74654837 2209.565
51.28458088 2209.7
52.9524241  2209.843
```

54.58318497 2210.019
56.91323325 2210.071
59.11583376 2210.298
61.02047283 2210.447
63.87619305 2210.702
66.27027284 2210.707
68.22353575 2210.938
69.96633034 2211.126
72.042818 2211.215
74.19043366 2211.4
75.54125156 2211.485
77.10069056 2211.596
77.58099151 2211.623
78.42140866 2211.768
78.69541596 2211.843
79.16880058 2211.83
79.52631422 2211.815
79.90841368 2211.827
80.31171258 2211.844
80.61730381 2211.915
81.03723833 2211.888
81.31054768 2211.972
81.60544597 2212.031
81.94493087 2212.037
82.26511988 2212.08
82.49018209 2212.172
83.04132363 2212.078
83.35277507 2212.22
83.60159027 2212.26
83.80159027 2212.154
83.93372656 2212.274
84.04610538 2212.5
84.2231308 2212.483
84.35113471 2212.64
84.94761522 2212.738
85.27176951 2212.69
85.41305291 2212.733
85.55833195 2212.41
85.71007516 2212.73
85.84410873 2212.814
85.99860469 2212.998
86.15868279 2213.034
86.28400239 2213.255
86.4293468 2213.166
86.59720984 2213.201
86.74121679 2213.252
86.8672525 2213.184
87.02141151 2213.228
87.14730829 2213.345
87.28086352 2213.346
87.42986688 2213.424
87.56987045 2213.546
87.72867851 2213.579
87.84595596 2213.596

87.99907356 2213.742
88.10517257 2213.843
88.29355516 2213.817
88.43664255 2213.773
88.55436255 2213.898
88.67839884 2213.942
88.81957249 2214.066
88.98527705 2214.106
89.12837491 2214.15
89.28612155 2214.245
89.44432395 2214.16
89.49145143 2214.103
89.6657156 2214.027
89.9287175 2214.411
90.18741617 2214.493
90.29528646 2214.702
90.45213352 2214.68
90.72531661 2214.805
91.15541079 2214.916
91.4604698 2215.014
92.06915526 2215.295
92.3257873 2215.313
92.60970454 2215.363
92.91130195 2215.427
93.19922555 2215.534
93.48851779 2215.669
93.78955932 2215.79
94.07622463 2215.83
94.38590995 2215.981
94.65061545 2215.972
94.95330341 2216.194
95.51428826 2216.224
95.80497709 2216.282
96.10551661 2216.39
96.29845442 2216.486
96.41656031 2216.432
96.60632332 2216.523
96.89044477 2216.576
97.19811342 2216.592
97.49420969 2216.654
97.84873755 2216.681
98.39292961 2216.644
99.42159476 2216.899
104.518175 2217.279
105.7503738 2217.393
107.8842307 2217.108
109.8114735 2217.757
111.9806586 2217.576
113.5528425 2218.137
115.2536896 2218.144
117.5601633 2218.352
119.4716151 2218.514
121.4106484 2218.695
123.4166327 2218.833

124.6273729 2218.963
126.5183674 2219.081

Profile 2

0 2209.539
2.003014229 2209.638
4.150833588 2209.844
5.974840441 2210.045
8.544183742 2210.29
8.554233618 2210.286
11.2141182 2210.464
13.53574263 2210.698
15.38715858 2210.844
17.19643827 2210.998
18.65236031 2211.175
20.09426773 2211.262
21.83511867 2211.538
23.4899096 2211.583
24.93107718 2211.723
25.58429843 2211.767
30.70587133 2212.161
31.59849051 2212.239
32.06325927 2212.219
32.66428007 2212.347
33.09941913 2212.14
33.60671391 2212.327
34.15643475 2212.405
34.49790949 2212.412
34.55247138 2212.45
34.92490661 2212.55
35.18566896 2212.582
35.56059962 2212.68
35.85085812 2212.742
36.20457694 2212.674
36.49283377 2212.817
44.71676871 2215.669
48.64164999 2217.331
49.26280375 2217.446
50.350019 2218.036
50.88102936 2218.24
51.06998703 2217.964
52.08895955 2218.399
52.55364546 2218.072
54.10786585 2218.272
56.15689928 2218.325
59.9105455 2218.814
62.00615329 2218.6
64.43733901 2219.145
66.01666323 2219.334
71.99834611 2219.734
74.69217313 2220.171

76.85926265 2220.379
81.08739994 2220.649
84.22804478 2220.936
86.11438542 2220.954
88.25416905 2221.024
90.25005507 2221.146
93.02710045 2221.367
97.27200386 2221.659

Profile 3

0 2208.325
2.781261765 2208.571
7.174054157 2208.932
10.19131931 2209.11
12.55501557 2209.25
15.93761176 2209.454
18.76598408 2209.642
21.36104555 2209.845
24.11906549 2210.006
26.85862257 2210.192
29.50710931 2210.412
31.71794806 2210.536
34.4690413 2210.775
36.49502378 2211.028
38.66428402 2211.338
40.19749796 2211.488
41.48490505 2211.624
42.53794351 2211.833
43.42546816 2212.03
44.25754087 2212.137
45.1269004 2212.252
45.82795818 2212.356
46.49518003 2212.532
47.3567414 2212.743
50.63799299 2213.466
51.49110787 2213.58
52.55629565 2213.732
53.83472164 2214.149
54.20744808 2214.287
54.68803314 2214.522
55.18589356 2214.75
56.00061928 2215.259
56.92371678 2215.577
57.65410435 2215.786
58.3450783 2215.923
59.01579806 2216.051
60.05979806 2216.249
61.07385773 2216.386
62.13917693 2216.572
63.00544767 2216.588
63.79157043 2216.626
65.58658046 2216.791
67.80748681 2216.92

69.5441091 2216.993
71.34320693 2217.144
72.83789118 2217.25
74.81423984 2217.396
76.32399081 2217.493
78.31152194 2217.65
80.6401825 2217.825
82.94356479 2217.982
84.61680178 2218.106
86.50378137 2218.321
88.58173445 2218.548
90.62417662 2218.623
92.52888657 2218.705
94.65738017 2218.946
96.98372193 2219.053
98.4527495 2219.181
102.661921 2219.483
105.6647574 2219.743
108.3143862 2220.038
110.4828774 2220.217
114.6119592 2220.553
117.3184588 2220.835
120.2107064 2221.051
123.1084811 2221.286
125.1635324 2221.453

Profile 4

0 2206.782
21.6898 2208.026
23.73656574 2208.183
25.44305453 2208.293
28.18213212 2208.426
29.75794207 2208.544
31.15897597 2208.623
33.24514806 2208.787
48.89931212 2209.378
50.73541233 2209.639
57.11463995 2210.35
59.57839258 2210.754
64.28449075 2210.991
65.96329568 2211.065
84.62004461 2212.106
85.45244175 2212.164
86.63345911 2212.291
88.8374666 2212.374
90.90845211 2212.522
92.48688995 2212.738
93.79917802 2212.804
95.47190544 2212.923

Profile 5

0	2247.74
2.292289031	2247.921
4.674831581	2247.873
6.722259478	2247.893
9.010693441	2248.091
11.06224139	2248.213
13.41342003	2248.33
15.43263374	2248.538
17.02429859	2248.7
19.14069222	2248.74
20.72702447	2248.872
22.51744928	2249.046
24.74958929	2249.375
26.43260384	2249.587
28.74457789	2249.735
30.72108112	2249.888
32.26924422	2249.942
34.24748309	2250.172
35.6822531	2250.373
37.43165414	2250.542
38.58666107	2250.706
40.1660828	2251.069
41.25383369	2251.201
42.7048268	2251.568
43.33074772	2251.699
43.87690246	2251.776
44.37826959	2251.898
44.76683747	2252.03
45.1658475	2252.158
45.51371529	2252.296
46.04341332	2252.511
46.47176131	2252.768
47.30641692	2253.019
47.87772157	2253.183
48.23775629	2253.314
48.80233135	2253.521
49.33099476	2253.907
50.02886079	2254.152
50.42391649	2254.248
51.41006303	2254.631
52.02019826	2254.731
52.54991611	2254.847
52.98236264	2254.979
53.64632423	2255.129
54.17335839	2255.213

54.68391201 2255.389
55.41013029 2255.567
56.15708478 2255.646
56.93542275 2255.767
57.66295076 2255.864
58.48095626 2256.076
59.06107435 2256.122
59.69240707 2256.23
60.2756463 2256.271
60.99468037 2256.389
61.67169219 2256.504
62.65069015 2256.645
63.41278463 2256.729
65.07176413 2257.058
66.28345551 2257.256
67.33056296 2257.367
68.35359424 2257.475
70.0368209 2257.697
71.40085976 2257.996
73.41007378 2258.365
74.24753721 2258.442
75.07598939 2258.663

Profile 6

0 2286.001
1.368073828 2286.384
2.165672725 2286.61
3.247405132 2286.942
4.321440513 2287.183
5.69778531 2287.533
7.080145973 2287.836
8.365301216 2288.126
9.585218016 2288.458
10.69204818 2288.751
11.82203092 2289.007
12.7888701 2289.26
14.09659675 2289.563
15.20312691 2289.875
16.42034054 2290.182
17.68320909 2290.507
18.76850445 2290.841
19.92982137 2291.124
21.07168389 2291.436
22.40219131 2291.749
23.57719514 2292.079
25.14690976 2292.359
26.31753694 2292.675
27.75977548 2292.999
28.95990256 2293.234
30.02406655 2293.448
31.75650212 2293.711
32.80479311 2293.952

33.82657831 2294.208
34.83298827 2294.419
36.0194574 2294.668
36.62475484 2294.818
37.15372365 2294.93
38.01945398 2295.085
38.65379301 2295.241
39.9959383 2295.519
41.00918112 2295.708
41.99963556 2295.984
42.78253849 2296.144
44.04024315 2296.21
44.64609461 2296.436
45.47267613 2296.648
45.98610577 2296.739
46.54707814 2296.959
47.17384445 2297.12
47.63102931 2297.304
48.24173792 2297.551
48.98337462 2297.665
49.71397711 2297.912
50.14062568 2298.075
50.72559833 2298.285
51.2870892 2298.398
51.60853593 2298.522
51.96606215 2298.674
52.4184171 2298.864
53.00943064 2299.013
53.47512152 2299.182
53.88522029 2299.262
54.35776764 2299.41
55.04368673 2299.63
55.41852003 2299.822
55.65000221 2299.938
56.05278379 2300.047
56.5091926 2300.175
56.94119375 2300.348
57.33260786 2300.472
57.94785577 2300.792
58.33044955 2300.901
58.78467087 2301.111
59.18832666 2301.207
59.6745005 2301.307
60.07182782 2301.459
60.51725458 2301.662
61.20038048 2301.802
61.62722237 2301.947
62.14308767 2302.094
62.67233241 2302.197
63.18115556 2302.307
63.65057648 2302.473
64.4660469 2302.777
64.93679949 2302.923
65.60644417 2303.028

66.16541913 2303.226
66.67605892 2303.377
67.18956549 2303.451
67.70312659 2303.566
68.1685479 2303.686
68.60887165 2303.842
69.0040425 2303.928
69.50532086 2304.009
69.89790207 2304.064
70.57414167 2304.213
71.04192153 2304.341
71.48449243 2304.443
72.02063607 2304.586
72.49844461 2304.676
73.31386106 2304.873
73.92482751 2305.078
74.85296813 2305.272
75.92622858 2305.548
76.99461521 2305.772
77.90604541 2306.013
78.73544579 2306.224
80.21492273 2306.56
81.45174608 2306.872
82.80099661 2307.187
84.25779104 2307.543
85.58785043 2307.86
86.82354174 2308.209
88.91935566 2308.689
90.52350341 2309.107
91.83463765 2309.404
93.33564065 2309.892
94.87296202 2310.319
96.53035335 2310.876
98.74362445 2311.386
100.4081643 2311.882
102.0038914 2312.292
103.3457756 2312.679
104.9299529 2313.07
106.2912791 2313.527
108.1988944 2314.048

Profile 7

0 2207.302
2.82587986 2207.527
6.01210427 2207.862
8.91757308 2208.133
11.9334625 2208.418
15.0689798 2208.693
17.7622672 2208.921
20.8930283 2209.1
23.9205319 2209.249
26.8587642 2209.453

30.0346968 2209.602
32.9421528 2209.769
35.8755852 2210.101
38.8139768 2210.471
41.8791071 2210.822
44.7397508 2211.058
47.7319092 2211.248
50.9356286 2211.573
52.6989646 2211.779
54.6111302 2212.172
56.6346884 2212.339
58.6327775 2212.727
60.6392234 2213.046
62.8804846 2213.254
64.7351288 2213.5
66.4226595 2213.612
68.7244825 2213.853
69.5825204 2214.072
70.5637737 2214.202
71.5376812 2214.37
72.5605058 2214.609
73.4489707 2214.867
74.5654742 2215.289
75.3355268 2215.552
76.5956272 2215.843
77.2770287 2216.109
78.3908065 2216.318
79.4398332 2216.63
80.4163740 2217.045
81.2218137 2217.384
82.0813676 2217.649
82.9254446 2218.108
83.9580772 2218.467
84.8480536 2218.914
85.8395252 2219.082
86.7303686 2219.246
87.8448874 2219.509
88.7484027 2219.636
96.8197962 2220.522
98.8305100 2220.525
107.739466 2220.581
109.853255 2220.619
112.354185 2220.755
114.204718 2220.813
116.827728 2220.925

Appendix D

Single Slip Diffusion Model

The single slip diffusion model was originally published in Regalla et al., 2007. It has since been modified with a simulation of the scarp decaying.

```
%%%%%%%%%%%%%%%%%%%%%%%%%%%%%%%%%%%%%%%%%%%%%%%%%%%%%%%
%%%%%%%%%%%%%%%
%                              Christine Regalla %
%                              last modified    %
%                              8/23/21          %
%                                        %
% function [Z, model_Z, model_t, RMS] = scarpdiffusion_modified2        %
%                                        %
% Foward in time cnetered in space, fully implicit, finite difference    %
% solution for 1-D diffusion of a topographic scarp. Reads a tab demited %
% text file of topographic profile data, in two columns of x (elevation) %
% and z (elevation) data points. Once text profile is entered once, the  %
% profile can be saved as a .mat file and reloaded in subsequent models. %
% Midpoint and regressions through lower and upper surfaces can be       %
% chosen graphically or entered  numerically.                  %
% A 'best fit' profile and 'best model age' are determined              %
% from a minima RMS fit between observed profile slopes and model slopes %
%                                        %
% Outputs:                                  %
%    Z = matrix of Z, for each timestep                        %
%    model_z = best fit model, elevation profile                 %
%    model_t = best fit model age (yrs)                      %
%    RMS = RMS fit for slopes for each model run                  %
%    ru = slope and intercept of regression through lower surface        %
%    rl = slope and intercept of regression through upper surface        %
%    ru_l = intersection point between lower fan surface and scarp face  %
%    rl_i = interdrction point between upper fan surface and scarp face  %
%                                        %
%%%%%%%%%%%%%%%%%%%%%%%%%%%%%%%%%%%%%%%%%%%%%%%%%%%%%%%
%%%%%%%%%%%%%%%
clear all; close all;
      %__________________________________________________%
      %SET MODEL PARAMETERS%
        K = 1.275/1000; %Diffusion consant (m^2/yr)
        ALPHA = 35;     %inital scarp angle (degrees)
        tfinal = 3e4;   %total run time in years
        dt=50;  %timestep
        dx = 0.25;  %x-interval used to discretize profile
      %__________________________________________________%

          %Convert to radians
          ALPHA = tan(ALPHA*pi/180);


 qq = (input('Import a) raw profile data (.txt)? or b) processed data file (.mat)? (a or b):     ', 's'));
 filename = (input('Enter the profile filename, with extension:     ', 's'));
 if qq == 'a'
   p=dlmread(filename);
   figure
   plot (p(:,1), p(:,2), '.b');
```

```
   %REVERSE ORIENTATION OF PROFILE IF RIGHT-FACING
   o = (input('Does the scarp face a)left or b)right? (a or b):     ', 's'));
   if o=='b'
      p2= [[p(2:end,1)-p(1:end-1,1);0], p(:,2)];
       for i=1:size(p,1)
          p3(i,:) = p2(end-i+1, :);
       end
      p2(:,:)=[cumsum(p3(:,1)), p3(:,2)];
      p=p2;
   end
   clf
   %}

   %DISCRETIZE PROFILE%
   x=[ceil(p(1,1)):dx:floor(p(end,1))]';
   z = interp1(p(:,1), p(:,2), x); %interpolate initial profile over dx
   hold on;
   h(1) = plot (p(:,1), p(:,2), '.b'); h(2) = plot (x,z, '-k');
   xlabel 'Distance Along Profile'; ylabel 'Height';
   legend (h, 'Profile points', 'Interpolated Profile', 'Location','SouthEast');


   %SELECT MIDPOINT AND REGRESS BOUNDING SURFACES
   q = (input('Do you wish to select midpoint and upper, lower surfaces a) graphically or b) by entering numerical
values? (a or b):     ', 's'));
   h=1; hu=1; hl= 1;
      %SELECT MIDPOINT%
      a='n';
      while a=='n'
         if q=='a'
            disp(' ')
            disp('Select the midpoint of the profile.     ')



% workaround text to make the ginput cursur to appear - a big in this
% Matlab version
 %pcolor (64*rand(100));
%legend('location','westoutside')
%legend('hide')
%


            midpt = ginput(1);
         elseif q=='b'
            midpt = input('Enter midpoint:  [x,z]    ');
         end
         %delete(h)
         d = sqrt((x-midpt(1)).^2 + (z-midpt(2)).^2);
         midpt = [x(d==min(d)), z(d==min(d))];
         plot(midpt(1), midpt(2), 'or')
         disp(' '); a=input('Would you like to keep the current midpt? (y/n)    ', 's');
      end

      %SELECT LOWER AND UPPER REGRESSION SURFACES%
      a='n';
      while a=='n'
         if q=='a'
            disp(' ')
            disp('Select range of points to use for lower surface regression, from left to right.     ')
            rl_range = ginput(2);
         elseif q=='b'
```

```
            rl_range = input('Enter bounding points on lower surface:  [left_x, left_z; right_x, right_z]    ');
        end
        %delete (hl);
        d = sqrt((x-rl_range(1,1)).^2 + (z-rl_range(1,2)).^2);
        ind = find (d==min(d));
        d = sqrt((x-rl_range(2,1)).^2 + (z-rl_range(2,2)).^2);
        ind(2) = find (d==min(d));
        rl = polyfit(x(ind(1):ind(2)), z(ind(1):ind(2)), 1);
        hl = refline(rl);
        disp(' '); a=input('Would you like to keep the regression? (y/n)    ', 's');

    end
        rl_range = [x(ind(1):ind(2)), z(ind(1):ind(2))];

    a='n';
    while a=='n'
        if q=='a'
            disp(' ')
            disp('Select range of points to use for upper surface regression, from left to right.     ')
            ru_range = ginput(2);
        elseif q=='b'
            ru_range = input('Enter bounding points on upper surface:  [left_x, left_z; right_x, right_z]    ');
        end
        %delete (hu);
        d = sqrt((x-ru_range(1,1)).^2 + (z-ru_range(1,2)).^2);
        ind = find (d==min(d));
        d = sqrt((x-ru_range(2,1)).^2 + (z-ru_range(2,2)).^2);
        ind(2) = find (d==min(d));
        ru = polyfit(x(ind(1):ind(2)), z(ind(1):ind(2)), 1);
        hu = refline(ru);
        disp(' '); a=input('Would you like to keep the regression? (y/n)    ', 's');
    end
        ru_range = [x(ind(1):ind(2)), z(ind(1):ind(2))];

    %CENTER PROFILE
    x=x-midpt(1); z = z-midpt(2);
    rl_range(:,1) = rl_range(:,1) - midpt(1); rl_range(:,2) = rl_range(:,2) - midpt(2);
    ru_range(:,1) = ru_range(:,1) - midpt(1); ru_range(:,2) = ru_range(:,2) - midpt(2);
    ru = polyfit(ru_range(:,1), ru_range(:,2), 1);
    rl = polyfit(rl_range(:,1), rl_range(:,2), 1);
    p(:,1) = p(:,1) - midpt(1); p(:,2) = p(:,2) - midpt(2);
    clf; hold on; h(1) = plot (x,z, '-k'); plot(0,0, 'or');

  disp(' ')
  q = (input('Save processed profile as .mat file? (y/n)       ', 's'));
  if q=='y'
     name = [input('Enter file name:   ', 's'), '.mat'];
     save (name, 'midpt', 'p', 'x', 'z', 'rl_range', 'rl', 'ru_range', 'ru')
  end
elseif qq=='b'
   load (filename)
   clf; hold on; h(1) = plot (x,z, '-k'); plot(0,0, 'or');
end
% CALCULATE INITIAL PROFILE
  rl_i = [(rl(2)/(ALPHA-rl(1))), (rl(2)/(ALPHA-rl(1)))*ALPHA];
  ru_i = [(ru(2)/(ALPHA-ru(1))), (ru(2)/(ALPHA-ru(1)))*ALPHA];
  Zo = [rl(1)*x((x<rl_i(1))) + rl(2); x(rl_i(1)<=x & x<=ru_i(1))*ALPHA  ;ru(1)*x(x>ru_i(1)) + ru(2)]; %initial profile:
Zo=mx+b
  h(2) = plot(x, Zo, '-r');    %plot initial profile
  xlabel 'Distance Along Profile'; ylabel 'Height';
  legend (h, 'Oberved Profile', 'Model Profile','Location','SouthEast');
  disp(' '); disp('Running diffusion model.....')
```

```
%
%RUN FTCS IMPLICIT SOLVER
   S=K*dt/dx^2;
   Z = [Zo, zeros(length(Zo), (tfinal/dt))];         %Z matrix for i timesteps
   A = (1+2*S)*eye(length(Zo)-2, length(Zo)-2) - S*diag(ones(1,length(Zo)-3), 1) - S*(diag(ones(1,length(Zo)-3), -1));
%Coefficient matrix
   for i=1:tfinal/dt;
      b = [Zo(2) + S*z(1); Z(3:end-2,i); Z(end-1,i) + S*z(end)];
      Z(:,i+1) = [z(1); A\b; z(end)];
   end

%CALCULATE RMS FIT between model and observed slopes,
%   calculated over a 5*dx point moving window
   t=0:dt:tfinal;        %time array (yrs)
   model_slopes = (Z(5:end, :)-Z(1:end-4,:))/(4*dx);
   obs_slopes = (z(5:end)-z(1:end-4))/(4*dx);
   for i=1:size(model_slopes, 2)
      RMS(i) = sqrt(sum((model_slopes(:,i)- obs_slopes).^2 /length(obs_slopes)));
   end
   model_Z = Z(:,(RMS==min(RMS(2:end))));% Z values for minimum RMS
   model_t = t(RMS==min(RMS(2:end)));  %best model t
 %}


%%
%b
% Animate plot %
   %set figure size
scrsz = get(0,'ScreenSize');
figm = figure('Position',[1 scrsz(4)*2/3 scrsz(3)*3/4 scrsz(4)*2/3], 'Name','Scarp Diffusion');
 xlabel 'Distance (m)'; ylabel 'Elevation';
axis([-10,10,-2,2]); hold on; %axis equal;
 h(1) = plot (p(:,1), p(:,2), '.-b', 'LineWidth', 3, 'MarkerSize', 15);
 h(2) = plot (x,Z(:,1), '--','Color', [0.4,0.4,0.4], 'LineWidth', 1.5);
 l = legend(h, 'Measured Profile', 'Initial Profile', 'Location', 'NorthWest');
 set(l, 'FontSize', 18);
 pause(2);


 M(1:15) = getframe (figm); m=16;

for i=2:2:size(Z,2)/6
h = plot(x,Z(:,i), '-r', 'LineWidth', 1.5);
tt = text(4,-0.5, ['Time = ', num2str(i*dt*10), ' Years'], 'FontSize', 18);
pause(1)

 M(m:m+11) = getframe (figm);  m=m+12;
delete(h); delete(tt);
end
plot(x,Z(:,i), '--r', 'LineWidth', 1.5);
plot(x,model_Z, '-.k', 'LineWidth', 1.5);
M(m:m+30) = getframe(figm);
%}
%%
%PLOT MODEL SCARP
   clf; subplot (2,1,1); hold on
   h(1) = plot(p(:,1), p(:,2), '.b');  %plot profile points
   h(2) = plot(x, Zo, '-r');    %plot initial profile
   h(3) = plot (x, model_Z, '-k');    %plot final Z
   axis ([p(1,1), p(end, 1), min(p(:,2))-1, max(p(:,2))+1]);
   xlabel 'Distance (m)', ylabel 'Height (m)'; title (filename)
   text (x(end)*13/24, (max(p(:,2))+1)*3/4, ['Model Age = ', num2str(model_t/1000), 'Kyr']);
```

```
    legend(h, 'Observed Profile', 'Initial Profile', 'Model Profile', 'Location', 'Southeast')

   %Calculate morphologic age and plot RMS:
    Kt = t.*K;
    best_Kt = Kt(RMS==min(RMS(2:end)))
    subplot (2,1,2); plot (Kt(2:end), RMS(2:end))
    hold on; h= plot(best_Kt, RMS(RMS==min(RMS(2:end))), '.k');
    xlabel 'Morphologic Age, KT (m^2)'; ylabel 'RMS'; title(filename);
    legend(h, ['Best Kt = ', num2str(best_Kt)]);
    disp(['For an K of ', num2str(K), '(m^2/yr) the best modeled age is....'])
    disp([num2str(model_t/1000), ' Kyr'])


%Save variables
disp(' ')
q = (input('Save variables as .mat file? (y/n)       ', 's'));
if q=='y'
    name = [input('Enter file name:   ', 's'), '.mat'];
    save (name)
end

%%%%%%%%%%%%%%%%%%%%%%%%%%%%%%%%%%%%%%%%%%%%%%%%%%%%%%%%%%%%%%%%%%%%%%%%%%%%%%%
%%Analytical solution
%center profile
%x_anl = x(:,1)-midpt*2;
%Z_anl = (11)* erf(x/(2*sqrt(D*23000))) + ru(1).*x(:,1);
%figure; hold on;
%h(1) = plot(x, Zo, '-r');    %plot initial profile
%h(2) = plot (x, model_Z, '--b');         %plot final Z
%h(3) = plot(x, Z_anl, '-k')
%h(3) = plot(x_anl+midpt*2, Z_anl+Zo(1), '--k');   %plot anl sol
%slop mid scarp
%dudx = polyfit (x(306/dx:336/dx, 1), x(306/dx:336/dx, 2), 1);
%slope = ~35 deg
```

Appendix E

Monte Carlo Simulation

The Monte Carlo Simulation is used to determine uncertainties on the single slip diffusion model.

```
%%%%%%%%%%%%%%%%%%%%%%%%%%%%%%%%%%%%%%%%%%%%%%%%%%%%%%%
%%%%%%%%%%%%%%%%
%                              Christine Regalla %
%                              last modified    %
%                              7/22/21          %
%                                        %
%                                        %
% This script will calcualte vertical separation, heave, throw, and      %
% fault slip from a topographic profile across a fault scarp. This       %
% code reads a tab demited text file of topographic profile data, which  %
% must be formatted in two columns of x (distance) and z (elevation)     %
% data points. Once text profile is entered, the profile can be saved as %
% a .mat file and reloaded in subsequent runs. Midpoint and regressions  %
% through lower and upper surfaces can be chosen graphically or entered  %
% numerically (ex. if they are known from field surveys or previous      %
% analyses).
%
% This script runs a Monte Carlo Simulation, where uncertianty in fault  %
% is determined by iterating this script N times. For each iteration,    %
% input script variables are randomly sected from a prescribe parameter  %
% space given by the uncertainty in fault dip, midpoint location, and    %
% upper and lower surface regressions. The output vertical separation,   %
% heave, and throw are reported with most litlely values and uncertainty %
% given the range of input values from the colletive set of model runs.  %
%
%                                        %
% Inputs:                                  %
%   filename.txt = tab delimited text file (without formatting)         %
%        containing x and z data for the topographic scarp profile    %
%                                        %
% Outputs:                                   %
%   VS = vertical separation, calculated as the difference between the  %
%        elevation of the projection of upper and lower surfaces at    %
%        the scarp midpoint                          %
                               %
%   ru = slope and intercept of regression through lower surface       %
%   rl = slope and intercept of regression through upper surface       %
%   ru_l = intersection point between lower fan surface and scarp face  %
%   rl_i = intersection point between upper fan surface and scarp face  %
%                                        %
%%%%%%%%%%%%%%%%%%%%%%%%%%%%%%%%%%%%%%%%%%%%%%%%%%%%%%%
%%%%%%%%%%%%%%%%
clear all; close all;  %clear all existing variables; close all existing plots
    %_______________________________________________%
    % SET SCRIPT VARIABLES %

      FAULTANGLE = 60;    %fault angle (degrees)  positive (+) faults dips have a slope that is
                    % positive in x,y, crtesian space; that is the fault plane slopes down to the left
                    % toward the negative x axis
      FAULTUNCERT = 10;      % +/- uncertainty (degree) in fault angle
      dx = 0.25;          % x-interval used to discretize profile (must be less than your data sample interval)

      nruns = 100;        % # of Monte Carlo Runs
```

```
          alpha = .05;       %confidence interval for regression uncertainty (e.g. .05 for 95%...2sigma, or .01 for
99%....3sigma)

        %_____________________________________________________%

             %Convert FAULTANLGE to dimensionless slope
              mf = tan(FAULTANGLE*pi/180);


    % READ IN INPUT TEXT FILE FILENAME.txt
    qq = (input('Import a) raw profile data (.txt)? or b) processed data file (.mat)? (a or b):     ', 's'));
    filename = (input('Enter the profile filename, with extension:     ', 's'));
    if qq == 'a'
       p=dlmread(filename);
       plot (p(:,1), p(:,2), '.b');

   %REVERSE ORIENTATION OF PROFILE IF RIGHT-FACING
       o = (input('Does the scarp face a)left or b)right? (a or b):     ', 's'));
       if o=='b'
          p2= [[p(2:end,1)-p(1:end-1,1);0], p(:,2)];
           for i=1:size(p,1)
              p3(i,:) = p2(end-i+1, :);
           end
          p2(:,:)=[cumsum(p3(:,1)), p3(:,2)];
          p=p2;
       end
       clf

   %DISCRETIZE PROFILE%
   x=[ceil(p(1,1)):dx:floor(p(end,1))]';
   z = interp1(p(:,1), p(:,2), x); %interpolate initial profile over dx
   hold on;
   h(1) = plot (p(:,1), p(:,2), '.b'); h(2) = plot (x,z, '-k');
   xlabel 'Distance Along Profile'; ylabel 'Height';
   legend (h, 'Profile points', 'Interpolated Profile', 'Location','SouthEast');


   %SELECT MIDPOINT AND REGRESS BOUNDING SURFACES
   q = (input('Do you wish to select midpoint and upper, lower surfaces a) graphically or b) by entering numerical
values? (a or b):     ', 's'));
   h=1; hu=1; hl= 1;
       %SELECT MIDPOINT%
       a='n';
       while a=='n'
          if q=='a'
             disp(' ')
             disp('Select the midpoint of the profile.     ')

       %{
       % workaround text to make the ginput cursur to appear - a bug in old
       % Matlab version
          %pcolor (64*rand(100));
       legend('location','westoutside')
       legend('hide')
       %}

             midpt = ginput(1);
          elseif q=='b'
             midpt = input('Enter midpoint:  [x,z]    ');
          end
          d = sqrt((x-midpt(1)).^2 + (z-midpt(2)).^2);
```

```
   midpt = [x(d==min(d)), z(d==min(d))];
   temppoint = plot(midpt(1), midpt(2), 'or');
   disp(' '); a=input('Would you like to keep the current midpt? (y/n)    ', 's');
   if a=='n'
      delete(temppoint)
   end
end


%SELECT LOWER AND UPPER REGRESSION SURFACES%
a='n';
while a=='n'
   if q=='a'
      disp(' ')
      disp('Select range of points to use for lower surface regression, from left to right.     ')
      rl_range = ginput(2);
   elseif q=='b'
      rl_range = input('Enter bounding points on lower surface:  [left_x, left_z; right_x, right_z]    ');
   end
   %delete (hl);
   d = sqrt((x-rl_range(1,1)).^2 + (z-rl_range(1,2)).^2);
   ind = find (d==min(d));
   d = sqrt((x-rl_range(2,1)).^2 + (z-rl_range(2,2)).^2);
   ind(2) = find (d==min(d));
   rl = polyfit(x(ind(1):ind(2)), z(ind(1):ind(2)), 1);

   hl = refline(rl);
   disp(' '); a=input('Would you like to keep the regression? (y/n)    ', 's');
   if a=='n'
      delete(hl)
   end

end
   rl_range = [x(ind(1):ind(2)), z(ind(1):ind(2))];

a='n';
while a=='n'
   if q=='a'
      disp(' ')
      disp('Select range of points to use for upper surface regression, from left to right.     ')
      ru_range = ginput(2);
   elseif q=='b'
      ru_range = input('Enter bounding points on upper surface:  [left_x, left_z; right_x, right_z]    ');
   end
   d = sqrt((x-ru_range(1,1)).^2 + (z-ru_range(1,2)).^2);
   ind = find (d==min(d));
   d = sqrt((x-ru_range(2,1)).^2 + (z-ru_range(2,2)).^2);
   ind(2) = find (d==min(d));
   ru = polyfit(x(ind(1):ind(2)), z(ind(1):ind(2)), 1);

   hu = refline(ru);
   disp(' '); a=input('Would you like to keep the regression? (y/n)    ', 's');
   if a=='n'
      delete(hu)
   end
end
   ru_range = [x(ind(1):ind(2)), z(ind(1):ind(2))];


%SELECT RANGE OF COORDINATES WHERE FAULT PLANE MAY INTERSECT SCARP FACE%
a='n';
while a=='n'
```

```
        if q=='a'
            disp(' ')
            disp('Select range of points that bound the possible intersection of the fault plane with the scarp face, from
left to right.     ')
            rf_range = ginput(2);
        elseif q=='b'
            rf_range = input('Enter bounding points on scarpface:  [left_x, left_z; right_x, right_z]    ');
        end
            d = sqrt((x-rf_range(1,1)).^2 + (z-rf_range(1,2)).^2);
            ind = find (d==min(d));
            d = sqrt((x-rf_range(2,1)).^2 + (z-rf_range(2,2)).^2);
            ind(2) = find (d==min(d));
            rfs = polyfit(x(ind(1):ind(2)), z(ind(1):ind(2)), 1);

            rf_range = [x(ind(1):ind(2)), z(ind(1):ind(2))];


            hf = plot(rf_range(:,1), rf_range(:,2), '-r', 'LineWidth', 2);
            disp(' '); a=input('Would you like to keep this range? (y/n)    ', 's');
        if a=='n'
            delete(hf)
            clear rf_range
        end
    end



    %CENTER PROFILE

    x=x-midpt(1); z = z-midpt(2);

    rl_range(:,1) = rl_range(:,1) - midpt(1); rl_range(:,2) = rl_range(:,2) - midpt(2);
    ru_range(:,1) = ru_range(:,1) - midpt(1); ru_range(:,2) = ru_range(:,2) - midpt(2);
    rf_range(:,1) = rf_range(:,1) - midpt(1); rf_range(:,2) = rf_range(:,2) - midpt(2);


        % Recalc y=mx+b for Upper surface
            x1 = ru_range(:,1);  z1 = ru_range(:,2);
            X1 = [ones(size(x1)) x1];
            [temp temp_int] = regress(z1,X1);
            ru(1)=temp(2); ru(2) = temp(1);
            ru_int(1,:) = temp_int(2,:); ru_int(2,:) = temp_int(1,:);

        % Recalc y=mx+b for Lower surface
            x1 = rl_range(:,1);  z1 = rl_range(:,2);
            X1 = [ones(size(x1)) x1];
            [temp temp_int] = regress(z1,X1);
            rl(1)=temp(2); rl(2) = temp(1);
            rl_int(1,:) = temp_int(2,:); rl_int(2,:) = temp_int(1,:);

        % Recalc y=mx+b for Fault scarp face:
            x1 = rf_range(:,1);  z1 = rf_range(:,2);
            X1 = [ones(size(x1)) x1];
            [temp temp_int] = regress(z1,X1);
            rfs(1)=temp(2); rfs(2) = temp(1);

    % PLOT SCARP
        clear h
        p(:,1) = p(:,1) - midpt(1);
        p(:,2) = p(:,2) - midpt(2);
        clf; hold on;
        h(1) = plot (x,z, '-k', 'LineWidth', 2); h(2) = refline(ru); refline(rl);
```

```
        xlabel ('Distance (m)')
        ylabel ('Elevtion (m)')

    %
     % Plot confidence intervals on upper surface:
        % http://www.real-statistics.com/regression/confidence-and-prediction-intervals/
        zhat = ru(2)+ru(1)*x;   %calcualte z values for regression line
        t = tinv(1-alpha/2,(length(x)-2)); %t value of distribution
        z_avg = mean(z); x_avg = mean(x);
        SX = sum((x-x_avg).^2); SY = sum((z-z_avg).^2);
        SXSY = sum((x-x_avg).*(z-z_avg)).^2;
        syx = sqrt((1/(length(x)-2))*(SY-(SXSY/SX)));  %std error in estimate ... Syx ... primary equation to solve
        CI = t*syx*sqrt(1/(length(x))+(x(:)-x_avg).^2/SX); % Calculate Confidence interval
        %calculate upper and lower confidence curves (linear)
        z_plus_CI = zhat + CI;
        z_minus_CI = zhat - CI;
        %plot confidence intervals
         plot(x,z_plus_CI,'r-.');
         plot(x,z_minus_CI,'r-.');

     % Plot confidence intervals on upper surface:
       % http://www.real-statistics.com/regression/confidence-and-prediction-intervals/

        zhat = rl(2)+rl(1)*x;   %calcualte z values for regression line
        t = tinv(1-alpha/2,(length(x)-2)); %t value of distribution
        z_avg = mean(z); x_avg = mean(x);
        SX = sum((x-x_avg).^2); SY = sum((z-z_avg).^2);
        SXSY = sum((x-x_avg).*(z-z_avg)).^2;
        syx = sqrt((1/(length(x)-2))*(SY-(SXSY/SX)));  %std error in estimate ... Syx ... primary equation to solve
        CI = t*syx*sqrt(1/(length(x))+(x(:)-x_avg).^2/SX); % Calculate Confidence interval
        %calculate upper and lower confidence curves (linear)
        z_plus_CI = zhat + CI;
        z_minus_CI = zhat - CI;
        %plot confidence intervals
         h(3) = plot(x,z_plus_CI,'r-.');
         plot(x,z_minus_CI,'r-.');

    %}



 %%% Save
  disp(' ')
  q = (input('Save processed profile as .mat file? (y/n)       ', 's'));
  if q=='y'
     name = [input('Enter file name:   ', 's'), '.mat'];
     save (name)
   end


% LOAD MAT FILE
% Load profile from Matlab variables if you are not laoding a text file
 elseif qq=='b'
    load (filename)
    clf; hold on; h(1) = plot (x,z, '-k', 'LineWidth', 2); h(2) = refline(ru); refline(rl);
          %plot confidence intervals
           h(3) = plot(x,z_plus_CI,'r-.');
           plot(x,z_minus_CI,'r-.');
    xlabel ('Distance (m)'); ylabel ('Elevation (m)')

 end
```

```
%%  MONTE CARO SIMULATION TO CALCULATE VERTICAL SEPARATION, SLIP, HEAVE, THROW

   % Equation for upper surface is:  y = mu*x + bu
   % Equation for lower surface is:  y = ml*x + bu
   % Equation for fault plane is:  y = mf*x + bf
      % Equation for the plane regressed through the scarp face is:
                        % y = rf(1)*x + rf(2)

   % where:
      % mu = slope of upper surface;  ru(1)
      % bu = y-int of upper surface; ru(2)
      % ml = slope of lower surface;  rl(1)
      % bl = y-int of lower surface; rl(2)
      % mf = slope of fault plane (= tan(FAULTANGLE))
      % bf = y-int of fault plane (right now it is 0)


   % therefore:  x = ((bu-bf)/(mf-mu));
   % and:        y = mf*((bu-bf)/(mf-mu)) + bf;


 for i=1:nruns

   % 1) Randomly generate fault angles
       F = (FAULTANGLE-FAULTUNCERT) + rand(1)* (2*FAULTUNCERT);
       FAULTANGLES(i) = F;
         mf = tan(F.*pi/180);
   % 2) Randomly generate a y-intercept for fault plane (given input range of coordiantes where fault can intersect the
fault scarp)
       % a) select point on scarp face where fault can intersect (choose an x value, fsx)
          fsx = rf_range(1,1) + rand(1)*(rf_range(end,1)-rf_range(1,1));
       % b) solve for the y -coordinate on the scarp face regression, using rf = (mf, bf);
          fsy = rfs(1)*fsx+rfs(2);
             %plot (fsx, fsy, '.r', 'MarkerSize', 30);
       % c) use point slope formula to calculate y-int for the fault plane, yield bf
             % y - yf = mf*(x - xf)
             % y = mf*x + (-mf*fsx + fsy)
             % so b = fsy - mf*fsx
          bf = fsy - mf*fsx;


    % plot "fault"
          dy = 10;  %'depth" to which fault will be plotted
          h(4) = plot([fsx, fsx-((dy)/(mf))], [fsy, fsy-dy], '--k');

   % 3) Randomly generate a regression line for upper surface

          %R = normrnd(mu,sigma)
          RU(1) = normrnd(ru(1), ((ru_int(1,2) - ru_int(1,1))/2));
          RU(2) = normrnd(ru(2), ((ru_int(2,2) - ru_int(2,1))/2));
          RUS(i,:) = RU;


    % 4) Randomly generate a regression line for lower surface

          RL(1) = normrnd(rl(1), ((rl_int(1,2) - rl_int(1,1))/2));
          RL(2) = normrnd(rl(2), ((rl_int(2,2) - rl_int(2,1))/2));
          RLS(i,:) = RL;
```

```
  % CALCULATE INTERSECTION BETWEEN FAULT PLANE AND UPPER / LOWER SURFACES
   % P1 = intersection (x,y) of upper surface and fault plane
     P1 = [(RU(2)-bf)/(mf-RU(1)); ((RU(2)-bf)/(mf-RU(1)))*(mf)+bf];
   % P2 = intersection (x,y) of lower surface and fault plane
     P2 = [(RL(2)-bf)/(mf-RL(1)); ((RL(2)-bf)/(mf-RL(1)))*(mf)+bf];


  % Where:
    % RU = a vector that contains the slope and intercept of the upper
        % surface regression line
    % RL = a vector that contains the slope and intercept of the lower
        % surface regression line

   % CALCUALTE THE INTERSECTION BETWEEN THE REGRESSION THROUGH THE FAULT
   % SCARP FACE AND THE UPPER / LOWER SURFACES
      % PA = intersection (x,y) of upper surface and scarp face
        PA = [(RU(2)-rfs(2))/((rfs(1))-RU(1)); (RU(2)-rfs(2))/(rfs(1)-RU(1))*rfs(1)+rfs(2)];
      % PB = intersection (x,y) of lower surface and scarp face
        PB = [(RL(2)-rfs(2))/((rfs(1))-RL(1)); (RL(2)-rfs(2))/(rfs(1)-RL(1))*rfs(1)+rfs(2)];

% CALCULATE VERTICAL SEPARATION
% VS is therefore the difference in z values between where a veritical line
% through the intersection point of the fault and the scarp face (fsx, fsy),
% intersects the upper and lower surfaces.  this is the difference between
% y(fsx) for the upper and lower surfaces

  VS(i) = (RU(1)*fsx+RU(2))-(RL(1)*fsx+RL(2));

  % Plot line along which vertical separation is measured
    h(5) = plot([fsx,fsx], [(RU(1)*fsx+RU(2)), (RL(1)*fsx+RL(2))], '-r');

%%%%%%%%%%%%%%%%%%%%%%%%%%%%%%%%%%%%%%
%CALCULATE DIP SLIP ALONG FAULT %
  fault_slip(i) = sqrt((P2(1,:)-P1(1,:)).^2 + (P2(2, :)-P1(2, :)).^2);
    %plot slip vector
    % plot([P2(1), P1(1)],[P2(2), P1(2)], '-g' );
%
% CALCULATE HEAVE AND THROW
  %Heave = the difference between the x vlaues of the points of
  %intersection between the fault plane and the upper/ lower surfaces
    Heave(i) = abs(P1(1))+abs(P2(1));

  %Throw = the difference between the y vlaues of the points of
  %intersection between the fault plane and the upper/ lower surfaces
    Throw(i) = abs(P1(2))+abs(P2(2));
%}

 end




 ave_vert_sep = mean(VS)
   stdev_vert_sep = std(VS)
 ave_slip = mean(fault_slip)
   stdev_slip = std(fault_slip)
 ave_heave = mean(Heave)
   stdev_heave = std(Heave)
 ave_throw = mean(Throw)
   stdev_throw = std(Throw)
```

```
 plotlegend = legend([h], 'Topo Profile', 'Surface Regressions', '95% Regression CI',...
     'Fault Plane', 'Vertical Separation', 'Location', 'Northeast');



%%
%Save variables
disp(' ')
q = (input('Save variables as .mat file, and plot as .fig? (y/n)       ', 's'));
if q=='y'
       corename = input('Enter file name:   ', 's');;
    name = [corename, '.mat'];
    save (name)
    save (name, 'midpt', 'p', 'x', 'z', 'rl_range', 'rl', 'ru_range', 'ru', 'rfs', 'rf_range',...
        'FAULTANGLES', 'VS','ave_vert_sep','stdtev_vert_sep', 'ave_slip', 'stdtev_slip', 'fault_slip',...
        'Heave', 'ave_heave', 'stdtev_heave', 'Throw', 'ave_throw', 'stdtev_throw');
    title(corename); saveas(gcf,corename);
end
```

Appendix F

CRONUS-Earth Online Calculator

CRONUS-Earth erosion rate calculator website:
https://hess.ess.washington.edu/math/v3/v3_erosion_in.html

Inputs to the CRONUS-Online calculator are described in:
http://hess.ess.washington.edu/math/docs/v3/v3_input_explained.html

Below is an example of the input tab delimited .txt file. This data can be typed into the data entry block to calculate erosion rates of each sample. Details of each input are explained in the above link.

```
Sample-1 44.406178        -115.176387      1911     std      0.05     2.65     0.963216426      0.00001  2023;
Sample-1 Be-10    quartz  1.406E+05        3.328E+03        07KNSTD;
Sample-2 44.236675        -114.997099      1930     std      0.05     2.65     0.970042475      0.00001  2023;
Sample-2 Be-10    quartz  6.451E+04        1.601E+03        07KNSTD;
Sample-3 44.108407        -114.860527      2004     std      0.05     2.65     0.985922152      0.00001  2023;
Sample-3 Be-10    quartz  2.043E+05        5.217E+03        07KNSTD;
Sample-4 44.080934        -114.869923      2020     std      0.05     2.65     0.99383122       0.00001  2023;
Sample-4 Be-10    quartz  2.173E+05        5.139E+03        07KNSTD;
Sample-5 43.870612        -114.652866      2225     std      0.05     2.65     0.965696154      0.00001  2023;
Sample-5 Be-10    quartz  2.899E+05        7.404E+03        07KNSTD;
Sample-6  43.787477       -114.568642      2051     std      0.05     2.65     0.987193726      0.00001  2023;
Sample-6 Be-10    quartz  3.103+E05        9.703E+03        07KNSTD;
Sample-7 43.782433        -114.503008      2003     std      0.05     2.65     0.948158503      0.00001  2023;
Sample-7 Be-10    quartz  1.459E+05        3.804E+03        07KNSTD;
```

First Line: Sample name, latitude, longitude, elevation, elevation handling flag, sample thickness, density, topographic shielding correction, erosion rate (number does not matter as a new one will be calculated), date of collection and a semicolon.

Second Line: Sample name, nuclide-mineral pair, [^{10}Be], [^{10}Be] uncertainty, Be-10 standardization and a semicolon.